



ORTA DOĞU TEKNİK ÜNİVERSİTESİ
FEN BİLİMLERİ ENSTİTÜSÜ MÜDÜRLÜĞÜ

CONSTRUCTION OF Z-SCAN SETUP AND INVESTIGATION OF
NONLINEAR OPTICAL PROPERTIES OF
ORGANIC ADDUCTS

A THESIS SUBMITTED TO
THE GRADUATE SCHOOL OF NATURAL AND APPLIED SCIENCES
OF
MIDDLE EAST TECHNICAL UNIVERSITY

BY

TOLGA ORÇUN ŞENGÖZ

IN PARTIAL FULFILLMENT OF THE REQUIREMENTS
FOR
THE DEGREE OF MASTER OF SCIENCE IN
CHEMISTRY

JANUARY 2023

Approval of the thesis:

**CONSTRUCTION OF Z-SCAN SETUP AND INVESTIGATION OF
NONLINEAR OPTICAL PROPERTIES OF
ORGANIC ADDUCTS**

submitted by **TOLGA ORÇUN ŞENGÖZ** in partial fulfillment of the requirements
for the degree of **Master of Science in Chemistry Department, Middle East
Technical University** by,

Prof. Dr. Halil Kalıpçılar
Dean, Graduate School of **Natural and Applied Sciences**

Prof. Dr. Özdemir Doğan
Head of the Department, **Chemistry**

Prof. Dr. Okan Esentürk
Supervisor, **Chemistry, METU**

Examining Committee Members:

Prof. Dr. Alpan Bek
Physics, METU

Prof. Dr. Okan Esentürk
Chemistry, METU

Prof. Dr. Seha Tirkeş
Chemical Eng, Atılım University

Assist. Prof. Dr. Çağatay Dengiz
Chemistry, METU

Assist. Prof. Dr. Antoine Marion
Chemistry, METU

Date: 18.01.2023

I hereby declare that all information in this document has been obtained and presented in accordance with academic rules and ethical conduct. I also declare that, as required by these rules and conduct, I have fully cited and referenced all material and results that are not original to this work.

Name Last name : **TOLGA ORÇUN ŞENGÖZ**

Signature :

ABSTRACT

CONSTRUCTION OF Z-SCAN SETUP AND INVESTIGATION OF NONLINEAR OPTICAL PROPERTIES OF ORGANIC ADDUCTS

Şengöz, Tolga Orçun
Master of Science, Chemistry
Supervisor: Prof. Dr. Okan Esentürk

January 2023, 82 pages

Nonlinear optical (NLO) concept became an important and attractive field due to potential applications in physics, chemistry, biology, and energy. There are many materials that can be investigated for their NLO properties such as 2D material and organic compounds. This thesis will cover the steps of construction, description of the optical parts used, experiences during construction processes, and verification of final setup with well-studied chemicals that are Tungsten disulfide and Methylene Blue. After verification of successful construction of the setup, nonlinear optical properties of organic compounds were measured. The studied compounds are based on the family of Tetracyanoethylene (TCNE) and Tetracyanoquinodimethane (TCNQ) based compounds, which are donor- π -acceptor (D- π -A) frameworks. Those frameworks have long conjugation connections, and electrons tend to exchange between acceptor and donor when excited. Thus, we expected and observed strong nonlinear properties. In this study, TCNE and TCNQ based compounds in DCM were explored by home-made Z-scan setup. The family of compounds may help us understand how distinctive donor structures influences nonlinear refractive index and nonlinear absorption coefficient of those compounds. Nonlinear refractive index and nonlinear absorption coefficients of these compounds are compared considering their conjugation length, HOMO-LUMO gaps as the donor groups have changed. It was observed that the TCNQ based compounds showed better nonlinear optical properties in general. In addition, we observed that

the nonlinear optical properties showed a strong correlation with good electron transfer quality of the donor group in both TCNQ and TCNE based compounds.

Keywords: Z-Scan technique, nonlinear optical properties, donor-acceptor groups, TCNE and TCNQ based compounds

ÖZ

Z-SCAN DÜZENEĞİNİN KURULUMU VE ORGANİK MADDELERİN LİNEER OLMAYAN ÖZELLİKLERİNİN İNCELENMESİ

ŞENGÖZ, TOLGA ORÇUN
Yüksek Lisans, Kimya
Tez Yöneticisi: Prof. Dr. Okan Esentürk

Ocak 2023, 82 sayfa

Fizik, Kimya, Biyoloji ve Enerji bilimlerindeki potansiyel uygulamaları nedeniyle, doğrusal olmayan optik özellikler kavramları sahada önemli hale gelmiştir. Bu konseptte 2 boyutlu malzeme, organik bileşikler gibi araştırılabilecek birçok malzeme bulunmaktadır. Bu çalışmada, Z-tarama kurulumu yapılmış ve kullanılan optik parçalar, yapım süreçlerindeki deneyimler ve son kurulumun Tungsten disülfid ve Metilen Mavisi ile doğrulanmasını içeren çalışma aşamaları anlatılacaktır. Doğrulamanın ardından organik bileşiklerin ölçümleri ve sonuçları açıklanacaktır. Tetrasiyanoetilen (TCNE) ve Tetrasiyanoquinodimetan (TCNQ) temelli bileşikler donör- π - alıcı (D- π -A) sistemlerdir. Bu tip bileşikler genellikle konjuge sistemlerdir ve bu sistemler yüksek yoğunlukta lazer ışını ile uyarıldığı zaman sistemde bulunan elektronlar, sistemde bulunan donör ile alıcı arasında transfer olmaya çok yatkındırlar. Bu durumdan dolayı bu bileşiklerin lineer olmayan özelliklerinin belirgin olması beklenmektedir. Bu tez de farklı donör gruplara sahip diklorometan (DCM) içinde çözülmüş TCNE ve TCNQ yapılarının kullanıldığı moleküllerin lineer olmayan optik özellikleri tamamen el ile kurulmuş Z-scan tekniği ile incelenmiştir. Bu moleküller, ayırt edici donör yapılarının bu bileşiklerin doğrusal olmayan kırılma indeksini ve doğrusal olmayan soğurma katsayısını nasıl etkilediğini anlamamıza yardımcı olabilir. Bu moleküllerin lineer olmayan kırılma indisi ve lineer olmayan absorpsiyon katsayıları, konjugasyon uzunlukları, donör grupları değişikçe HOMO-LUMO enerji farkı dikkate alınarak karşılaştırıldı ve tartışıldı. TCNQ temelli bileşiklerinin genel olarak daha iyi lineer olmayan optik özellikler gösterdiği

gözlendi. Ek olarak, doğrusal olmayan optik özellikler hem TCNQ hem de TCNE yapılarının kullanıldığı moleküllerin donör grubunun iyi elektron transfer kalitesi ile güçlü bir korelasyon gösterdiğini gözlemledik.

Anahtar Kelimeler: Z-scan tekniği, lineer olmayan optik özellikler, donör ve alıcı gruplar , TCNE ve TCNQ temelli bileşikler

To the journey

ACKNOWLEDGMENTS

Firstly, I'd like to express my thanks to patient and supportive supervisor, Prof Dr Okan Esentürk who has supported me throughout this research project. I am extremely grateful for our friendly chats at the end of our meetings and your personal support in my academic and business endeavors. In addition to that, I would like to thank Kübra Erden and Başak Karagöllü from Dengiz's research group for the samples. Finally, I would like to thank to my Family for their valuable support.

TABLE OF CONTENTS

ABSTRACT	v
January 2023	v
ÖZ	vii
ACKNOWLEDGMENTS	x
TABLE OF CONTENTS	xi
LIST OF TABLES	xiv
LIST OF FIGURES	xv
LIST OF SYMBOLS	xviii
1 INTRODUCTION	1
1.1 Aim of The Study	2
1.2 Theory of nonlinear light-matter interaction	3
1.3 Self-focusing (nonlinear refraction)	4
1.4 Nonlinear Absorption	5
1.5 Saturable absorption	6
1.6 Reverse saturable absorption.....	7
1.7 The Z-scan technique	8
1.8 Theory of nonlinear refraction	11
1.8.1 Gaussian beam at the sample	12
1.8.2 Introducing the phase shift.....	12

1.8.3	Transmittance into aperture	14
1.8.4	Nonlinear absorption	15
1.8.5	Factors that affect the nonlinear optical properties	16
2	EXPERIMENTAL.....	19
2.1	Z-SCAN system setup overview	20
2.2	Main parts of the system with their properties	21
2.2.1	Lasers.....	21
2.2.2	Quarter waveplate and Glan Thompson polarizer.....	23
2.2.3	Lenses.....	23
2.2.4	Motorized stage.....	24
2.2.5	Detectors.....	25
2.2.6	Data acquisition and analysis.....	26
2.2.7	Nonlinear refraction in cuvette material	30
2.2.8	Detector Area	30
2.2.9	Sample preparation	31
2.2.10	Optimization studies	33
2.2.11	Experiences from past to present on constructed setup.....	37
3	RESULT and DISCUSSION.....	43
3.1	Verification of constructed setup with literature	43
3.2	Introduction of organic push-pull compounds.....	48
3.3	HOMO-LUMO gap of TCNQ and TCNE based compounds	49
3.4	Sample Preparation and UV-VIS spectra of the compounds.....	51
3.5	Z-scan measurements of TCNE and TCNQ with alkynes substituted by electron-rich diethyl aniline and polycyclic aromatic hydrocarbon	53

3.5.1	Compound 1.1	53
3.5.2	Compound 1.2.....	55
3.5.3	Compound 2.1.....	57
3.5.4	Compound 2.2.....	59
3.5.5	Compound 3.1	61
<u>3.5.6</u>	Compound 3.2.....	63
3.6	Comparative discussions of TCNQ and TCNE based compounds	65
3.7	Additional studies.....	70
CHAPTER 4	75
4	CONCLUSION	75
	REFERENCES	77

LIST OF TABLES

Table 1. The equipment of Z-scan system.....	20
Table 2. The equipment of Z-scan system (Cont'd).....	21
Table 3 Extracted setup parameter	45
Table 4. Nonlinear refractive index and absorption coefficient of methylene blue.	47
Table 5. Extracted setup parameter along with the setup parameters of the instrument used for data collection.....	48
Table 6 HOMO-LUMO and ESP map. Reprinted from [52] with permission	50
Table 7 HOMO-LUMO gap for the compounds	51
Table 8 General view of compounds for comparison	65
Table 9. Results of 800 nm laser measurements for every compounds	66
Table 10 Results of 800 nm laser measurements for every compounds(con't).....	67
Table 11. Results of 632.8 nm laser measurements for every compounds	67
Table 12. HOMO-LUMO gap energies.....	69
Table 13. Nonlinear absorption and refractive index values of TCNQ attached NLOphores.	72
Table 14. Nonlinear absorption and refractive index values of TCNE attached NLOphores.	74

LIST OF FIGURES

Figure 1.1 Effects of nonlinear medium on laser beam shape	4
Figure 1.2 A schematic representation of a) single photon absorption and b) two photon absorption.....	6
Figure 1.3 Schematic representation of saturable absorption ¹⁶	6
Figure 1.4 An example for observation of saturable absorption on data	7
Figure 1.5 Schematic representation of reverse saturable absorption.....	7
Figure 1.6 Constructed z-scan setup	9
Figure 1.7 Difference between sign of the nonlinear refractive index.....	10
Figure 1.8 open aperture measurement setup.....	10
Figure 1.9 A) close aperture data B) open aperture data C) ratio, A/B	11
Figure 1.10 Propagation of gaussian beam along the z direction.....	12
Figure 1.11 Representation of $\Delta T_p - v$	15
Figure 1.12 results of a) multi photon absorption, reverse saturable absorption, and b) saturable absorption.	15
Figure 2.1 Z-Constructed final Z-scan setup	19
Figure 2.2 800nm laser source	22
Figure 2.3 632.8 He-Ne laser source.....	22
Figure 2.4 a) Glan Thompson polarizer b) working principle of quarter waveplate ⁵²	23
Figure 2.5 Arduino Uno	24
Figure 2.6 Motorized stage	25
Figure 2.7 a) S120C Photodiode Power Sensor and b) FDS100-CAL - Calibrated Si detector.....	25
Figure 2.8 Tektronix MS4101.....	26
Figure 2.9 PM100D digital handheld optical power and energy meter.....	26
Figure 2.10 Optical power monitor software	27
Figure 2.11 An example of a) a raw and b) normalized data.....	28

Figure 2.12 Detector area	31
Figure 2.13 Spin coating.....	32
Figure 2.14 WS ₂ measurements in different laser power.	33
Figure 2.15 An example of strong a) nonlinear absorption and b) nonlinear refractive index response of WS ₂ at 40 mW	34
Figure 2.16 An example of successfully collected data.	35
Figure 2.17 Example of a) closed aperture measurement and b) open aperture measurement with error bars.	36
Figure 2.18 First constructed setup	37
Figure 2.19 working principle of Pockels.	38
Figure 2.20 Schematic drawing of working principle of pulse picker system	38
Figure 2.21 Collected two pulse in our system.	39
Figure 2.22 Manual stage	39
Figure 2.23 nonlinear refractive index measurement with manual stage.....	40
Figure 2.24 Lenses, manual stage, and detector.....	40
Figure 2.25 Collected data with lenses that is located in front of detector	41
Figure 3.1 Experimental for a) nonlinear refractive index and b) nonlinear absorption coefficient of WS ₂ films.	44
Figure 3.2 a) Close and b) open aperture measurements of MB	46
Figure 3.3 UV-VIS spectrum of a) TCNQ and b) TCNE with alkynes substituted by electron-rich diethyl aniline and polycyclic aromatic hydrocarbons compounds.	52
Figure 3.4 Molecular structure and fragmentation of compound 1.1.....	53
Figure 3.5 a) Closed and b) open aperture Z-scan measurement results of 0.2 mM compound 1.1 in DCM at 632.8 nm.	54
Figure 3.6 a) Closed and b) open aperture Z-scan measurement results of 0.2 mM compound 1.1 in DCM at 800 nm.....	54
Figure 3.7 Molecular structure and fragmentation of compound 1.2.....	55
Figure 3.8 a) Closed and b) open aperture Z-scan measurement results of 0.2 mM compound 1.2 in DCM at 632.8nm	56

Figure 3.9 a) Closed and b) open aperture Z-scan measurement results of 0.2 mM compound 1.2 in DCM at 800 nm	56
Figure 3.10 molecular fragmentation of compound 2.1.....	57
Figure 3.11 a) Closed and b) open aperture Z-scan measurement results of 0.2 mM compound 2.1 in DCM at 632.8 nm.	58
Figure 3.12 a) Closed and b) open aperture Z-scan measurement results of 0.2 mM compound 2.1 in DCM at 800 nm	58
Figure 3.13 molecular fragmentation of compound 2.2.....	59
Figure 3.14 a) Closed and b) open aperture Z-scan measurement results of 0.2mM Compound 2.2 in DCM at 632.8 nm.....	60
Figure 3.15 a) Closed and b) open aperture Z-scan measurements of 0.2 mM compound 2.2 in DCM at 800 nm.	60
Figure 3.16 molecular fragmentation of compound 3.1.....	61
Figure 3.17 a) Closed and b) open aperture Z-scan measurements of 0.2 mM Compound 3.1 in DCM at 632.8 nm.....	62
Figure 3.18 a) Closed and b) open aperture measurements of 0.2 mM Compound 3.1 in DCM at 800 nm	62
Figure 3.19 molecular fragmentation of compound 3.2.....	63
Figure 3.20 a) Closed and b) open aperture Z-scan measurement result of 0.2 mM Compound 3.2 at 632.8 nm.....	64
Figure 3.21 a) Closed and b) open aperture Z-scan measurement results of 0.2 mM Compound 3.2 800 nm.....	64
Figure 3.22 Nonlinear absorption and refractive index measurements of TCNQ attached NLOphres	72
Figure 3.23 Nonlinear absorption and refractive index measurements of TCNE attached NLOphres	73

LIST OF SYMBOLS

DC:	Direct current
P:	Polarization
ϵ_0 :	Dielectric susceptibilities
X:	Linear susceptibility
E:	Electric field
N:	Molecule number in per unit volume
W:	Frequency
n_0 :	Linear refractive index
n_2 :	Nonlinear refractive index
α :	Linear absorption
β :	Nonlinear absorption
γ :	Three photon absorption
O:	Four photon absorption
Z:	Position of sample with respect to the focal position
Z_0 :	Rayleigh range
T(z):	Transmittance of the sample at Z
$w(z)$:	Beam radius
w_0 :	Beam waist at focus
$\Delta\varphi$:	Phase shift

L_{eff} : Effective sample thickness.

L: Sample thickness

S: Fraction of beam transmitted by the aperture

$I(z)$: Irradiance (power per unit area)

I_0 : Intensity at focus

$\Delta T_{\text{p-v}}$: Peak and valley in transmission

CW: Continuous wave

BS: Beam splitter

D: Detector

NLO: Nonlinear optical properties

mW: MilliWatt

MHz: MegaHertz

TCNE: Tetracyanoethylene

TCNQ: Tetracyanoquinodimethane

mM: Millimolar

nm: Nanometer

DCM: Dichloromethane

CHAPTER 1

INTRODUCTION

After the invention of the laser in the 1960s, people start to perform investigation nonlinear optical materials. Those materials have nonlinear response under high intense laser beam and first demonstration of the nonlinear effects of material was made by John Kerr in 1875.¹ He reported that when strong Direct Current (DC) field is applied to a material, its refractive index did change. This phenomenon is known as Kerr effect. Friedrich Pockels also performed studies in 1894 about nonlinear phenomena.²

Nonlinear optical (NLO) materials are crucial for the development of advanced modern technology, including terahertz (THz) generation, higher harmonic generation, optical switching, communication, signal processing and optical limiting.³ Zhou Yang et al introduces novel stilbazolium salt called DSTMS (4-N,N-dimethylamino-4'-N'-methylstilbazolium 2,4,6-trimethylbenzenesulfonate) with excellent crystal growth characteristics and outstanding second-order nonlinear optical qualities.⁴ It is grown as thin film and it is stated that DSTMS has significant non-linear optical susceptibilities, according to nonlinear optical measurements and it is a good crystal for broad band THz waves. One of the most practical uses for nonlinear optical properties is optical limiting. It may shield the human eye and photosensitive parts of delicate optical instruments from damage due to the powerful light radiation. This way a potentially harmful laser beam is greatly attenuated by optical means.⁵

Many photon technologies have been realized and developed as a result of nonlinear optics, which may also be utilized to process optical signalling more quickly. Large optical nonlinearities are essential for the successful use of novel nonlinear optical materials with ultrafast reaction times, great resistance to bulk and surface laser damage, and low two-photon absorption. These nonlinear materials are also often employed in waveguide applications. NLO properties of organic compounds is important. It has been shown that organic NLO materials have several benefits, including extremely high molecular hyperpolarizabilities, a wide variety of structural options, and ease of processing.⁶ Due to their high and quick nonlinearities as well as their general ease of processing and integration into optical systems, organic materials started to emerge as key targets of choice for nonlinear optical applications by the middle of the 1980s. Additionally, organic substances have the benefit of being tailorable. By altering the chemical structure, the NLO qualities can be fine-tuned.

Briefly, NLO properties of materials have wide application area and working with organic compounds is practical way in NLO concept. In this thesis, construction of a Z-scan setup and NLO properties of selected organic compounds will be investigated and discussed.

1.1 Aim of The Study

Main purpose of this study is to construct a Z-scan instrument and use of the instrument for the nonlinear property characterization of organic materials. First part of the study includes: 1) design of the Z-scan optical system, 2) obtaining all the optical, optomechanical, mechanical, electrical components needed for the successful construction of the instrument, 3) setting-up the instrument, 4) characterizing, optimizing, and testing the instrument, 5) verification of the setup with collecting data from compounds that has known nonlinear optical properties. After successful construction of the setup, its application on organic compounds for NLO characterization will be performed and the results will be discussed.

1.2 Theory of nonlinear light-matter interaction

Polarization is important property for the nonlinear optical phenomena because it varies with electric field magnitude. Polarization (\mathbf{P}) under the influence of electric field (\mathbf{E}) is given in eq 1.1 [7-8]

$$\mathbf{P}(\mathbf{E}) = \epsilon_0 (X^1 \mathbf{E} + X^2 \mathbf{E}\mathbf{E} + X^3 \mathbf{E}\mathbf{E}\mathbf{E} + X^4 \mathbf{E}\mathbf{E}\mathbf{E}\mathbf{E} + \dots) \quad 1.1$$

here, ϵ_0 is dielectric susceptibility and $X^{(n)}$ are coefficients that are special characteristic elements for every material for different order of electric field interactions. $X^{(1)}$ is the linear susceptibility and is a complex number that consist of real part and imaginary part. While real part has correlation with linear refraction index, n , imaginary part has correlation with linear absorption coefficient, α . The coefficients, $X^{(n)}$ with n greater than 1 indicate the higher order susceptibilities, which are considered in nonlinear processes. Because of their relatively low strengths in general, they are not considered for weak field interactions. The relative intensities of the next two higher order susceptibilities are typically on the order of 10^{-10} cm/V for $X^{(2)}$ and 10^{-17} cm²/V² for $X^{(3)}$. Therefore, high intensity light is necessary for higher order polarizations contributions. $X^{(n)}$ are tensors. They take into consideration the polarization of the incidence electric field relative to the orientation because the medium is anisotropic and hence responds differently to different polarization directions of the incident fields.

According to the order of the susceptibilities ($X^{(n)}$), different processes take places during light matter interaction. For example, $X^{(1)}$ defines two-wave interaction, $X^{(2)}$ define three-wave interaction, $X^{(3)}$ four-wave and so on. For the three-wave interaction, two waves that includes two frequencies w_1 and w_2 enter the phase and one wave with frequency w_3 leaves or the opposite situation can take place. During those interaction, momentum, angular momentum, and energy must be conserved. Thus, energy conservation means that $w_3=w_1+w_2$ or $w_3=w_1-w_2$. For the degeneracy case, second harmonic generation takes place because two equal frequencies enter the medium, $w_3=2w_1$. [9-10-11] In addition to that, degenerate frequency means only

one frequency laser is interacting with matter, as we have used in our Z-scan setups. Thus, for the term with $X^{(3)}$ four-wave interaction is needed, and if all three waves are the same it is called as third harmonic generation that can be express as ($3\omega_1=\omega_1+\omega_1+\omega_1$). In some cases, incident and exiting wave can have the same frequency and nonlinear phenomena takes place, $X^{(3)}$ term must be considered for example, $\omega_4=\omega_1-\omega_1+\omega_1=\omega_1$ and the lower term cannot be described. Self -focusing that will be discussed next, can be given as an example for this case.

1.3 Self-focusing (nonlinear refraction)

One of the nonlinear processes is self-focusing. As stated in section 1.1 at least a four-wave interaction must occur. Therefore, $X^{(2)}$ can be neglected because it has no effect on self-focusing and higher terms are contributing in very high intensities.¹² Thus the polarization equation becomes

$$\mathbf{P}(\mathbf{E}) = \epsilon_0(X^1\mathbf{E} + X^3\mathbf{E}\mathbf{E}\mathbf{E}) \quad 1.2$$

$$n = n_0 + n_2 (\mathbf{E} \cdot \mathbf{E}) = n_0 + \Delta n \quad 1.3$$

Self-focusing can be understood by the equation 1.5. Here, refractive index is dependent on the square of the incoming electric field. Therefore, refractive index change, Δn relative to n_0 is a function of the intensity, $I(r)$. (Figure 1.2)

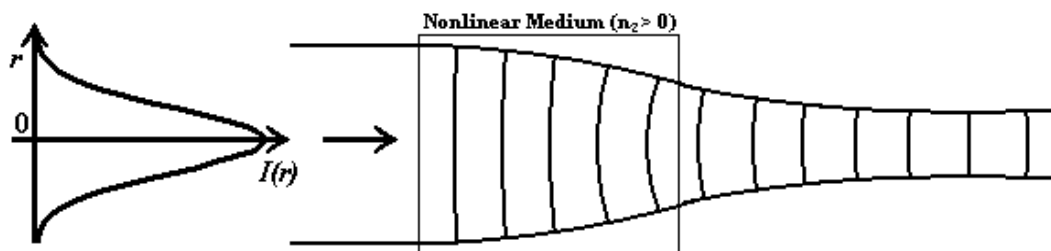


Figure 1.1 Effects of nonlinear medium on laser beam shape
Intensity of the incident laser light with gaussian beam shape has higher intensity at the center and decays in the flanks of the pulse. Therefore, refractive index change of the material would be bigger at the center of the

pulse that leads to a strong phase change $\Delta\phi$, hence Δn , of the laser pulse. As a result, material starts to behave like a lens. This is shown in Figure (1.1). In addition to that, self-focusing has sign that shows the place of the focusing. If $n_2 > 0$, focusing occurs at the edges of the medium (self-focusing) and if $n_2 < 0$, then defocusing will occur in the material.

1.4 Nonlinear Absorption

Beer's law can be applied to model the linear absorption where low intensity of light interacts with the matter.

$$I(z) = Ie^{-a(\omega)z} \quad 1.4$$

here, $a(\omega)$ is the linear absorption, I is the incident intensity, z is the depth of propagation for the medium that light matter interaction takes place, and intensity at position z in a medium is $I(z)$. Beer's law can be considered as a solution for the differential equation about how intensity of light decreases with the change in propagation depth in a medium while a is a fix:

$$\frac{\partial I}{\partial z} = -a(\omega)I \quad 1.5$$

When multi photon effect are present higher order terms must be included.^[13-14]

$$\frac{\partial I}{\partial z} = -a(\omega)I - \beta(\omega)I^2 - \gamma(\omega)I^3 - O(\omega)I^4 \quad 1.6$$

Symbol for two photon absorption is $\beta(\omega)$, symbol for three photon absorption is $\gamma(\omega)$, symbol for four photon absorption is $O(\omega)$. Basically, meaning of two photon absorption is exciting electron from ground state to excited state by using two photons. First photon excites the electron from ground state to a virtual state or to a real intermediate state¹⁵. Second photon excites the electron from there to the final excited state. In the three photons absorption, electron is excited with three photons from ground state to excited state.

Those phenomena are represented in the Figure 1.2. As a result, those are nonlinear phenomena's that are observed under high intense laser beam. However, there are saturable absorption and reverse saturable absorption that can be considered as nonlinear phenomena and they will be explained in the next sections.

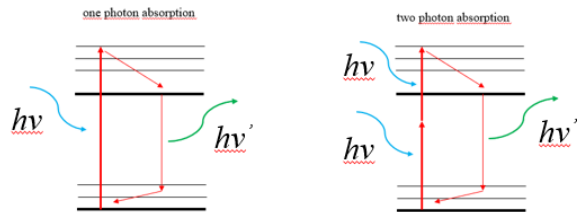


Figure 1.2 A schematic representation of a) single photon absorption and b) two photon absorption

1.5 Saturable absorption

Saturable absorption is a nonlinear absorption process. Under high intensity, excited electron can lead to saturation of excited state, and this situation limits interaction of light with electron in the ground state.¹⁶ Due to no interaction, an increase in transmittance is observed. Saturable absorption is represented in Figure 1.3 and reflection of saturable absorption in data also is given in Figure 1.4

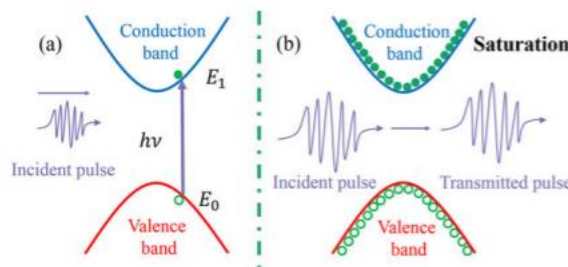


Figure 1.3 Schematic representation of saturable absorption¹⁶

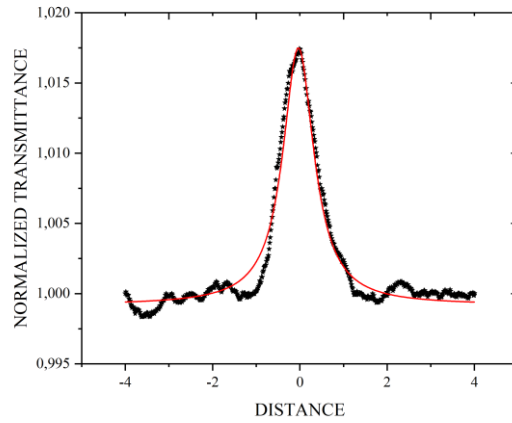


Figure 1.4 An example for observation of saturable absorption on data

1.6 Reverse saturable absorption

Reverse saturable absorption that is illustrated in Figure 1.5 is also a nonlinear process. If electrons are excited from the virtual state rather than the ground state, it is called as reverse saturable absorption. In this phenomena, cross section of the excited state absorption is larger than the ground state absorption.¹⁷

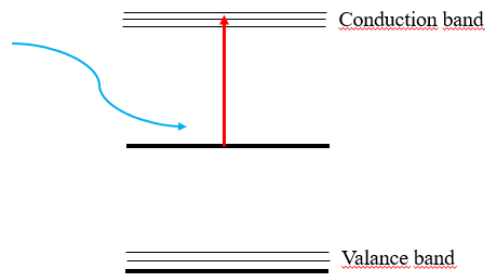


Figure 1.5 Schematic representation of reverse saturable absorption

1.7 The Z-scan technique

In the literature, there are several techniques to measure nonlinear optical properties of material such as four wave-mixing, Z-scan, nonlinear imaging and beam deflection. Four wave mixing is a technique to determine third order susceptibility. Basically, while three laser beams (k_1 k_2 k_3) propagate into nonlinear optical media, output measured with detector. It can calculate as $k_s = k_3 \pm (k_1 - k_2)$. Nonlinear imaging technique involves a phase object, a round film with a radius of L_p coated on a round glass-made substrate (referred to as the aperture) of a larger radius R_a], a pair of confocal lenses and a CCD camera, placed in sequence³. By locating the nonlinear sample at the confocal point (i.e., the Fourier plane) of both lenses, they measured the intensity distribution distortion of the top-hat incident laser beam induced by the sample's nonlinearity with the CCD camera. A polarization-resolved beam deflection technique is used to separate the bound-electronic and molecular rotational components of nonlinear refractive transients of molecular gases.¹⁷

In this thesis, Z-scan technique was chosen for its simplicity, easy applicability, easy integration our optical table. Basic principle of the Z-scan technique is that a sample is moved through a focal point of a gaussian laser beam. The light enters the sample along the surface normal, thus along the Z-axis, which is the interaction axis. This gives the name to the technique. As the sample is moving along the Z-axis and passes the focus of the beam, interaction between light and matter is varied because of the intensity differences at and close to the focus and the other places. As the sample is moved along the Z-axis and through the focus¹⁸, transmitted power through the sample as a function of sample position (Z-position) is recorded to get the information about the light matter interaction. This information includes nonlinear refractive index and nonlinear absorption coefficient of the sample. Such interactions as stated would only be possible if the intensity of the light is strong enough, such as at and close to the focus of the beam. To collect data about nonlinear refractive index of a sample, an aperture is placed in front of the detector, and it is called closed aperture measurement and detector measures the transmitted light intensity or power.

In this way, measurement become sensitive to spreading of beam (defocusing) or focusing and to phase change of the light. A simple setup configuration is shown in Figure 1.6

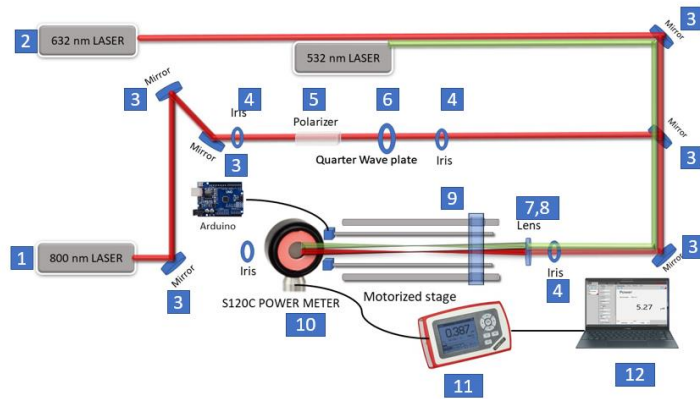


Figure 1.6 Constructed z-scan setup

In the constructed setup, S120C power meter is the detector to measure light intensity or power. If there is an aperture in front of the detector, then nonlinear refractive index measurement is made. If there is no aperture, then nonlinear absorption coefficient measurement is made. As sample is moving, a sample that shows nonlinear refraction will behave as lens causing a change in focal point. For example, a material having thickness less than Rayleigh length, z_0 and having negative refractive index. Here, the sample with those features has negligible nonlinear refraction when it is away from the focus because of the low intensity of the laser beam. When sample get closer to the focal point it will be acting as negative lens and spot size becomes smaller (see Figure 1.7). As a result of this, transmitted light intensity through the aperture is increased thus causes an increase of the signal on the detector. The signal increases further as the sample moves towards the focus. When the sample is just behind the focus possibly the maximum transmittance is observed, and maximum signal is obtained on the detector. This maximum transmittance (peak) decays suddenly after sample passes the focus and minimum transmittance (valley) is obtained as sample moves away from the focal point. Reason for the minimum transmittance is maximum divergence of the laser beam.

Finally, as sample gets closer to the detector signal returns to the original value. Figure 1.7 is representing an example response of the intensity change as the sample is moved for both positive and negative nonlinear index. Sign of the nonlinear refractive index can be observed from the plot.

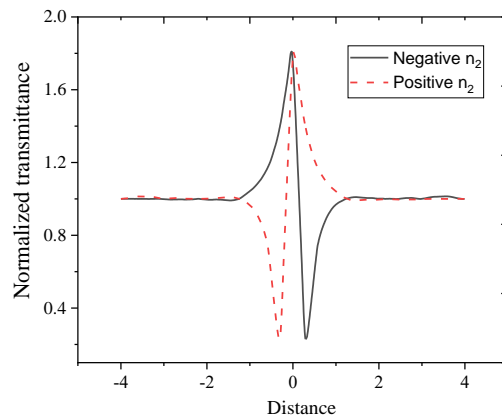


Figure 1.7 Difference between sign of the nonlinear refractive index

Closed aperture measurement is not enough as its own. For better understanding of the materials' nonlinear behavior, it is better to also measure the nonlinear absorption coefficient of the material.

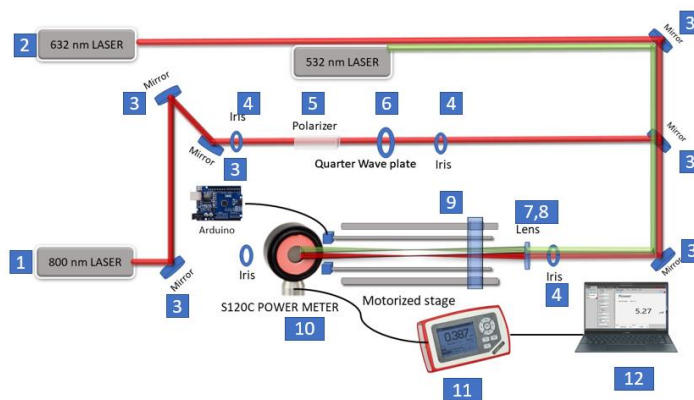


Figure 1.8 open aperture measurement setup

To determine the nonlinear absorption coefficient, aperture in front of the detector must be removed to collect all transmitted light all the time during the measurement without a loss. This is called open aperture measurement.²⁰ (see Figure 1.8) The light that is measured is then only dependent to nonlinear absorption and enables to figure out the nonlinear absorption coefficient of a material. After all close and open aperture measurements are performed, close aperture measurement data is divided by open aperture measurement data to figure out nonlinear refractive index that is illustrated in Figure 1.9.

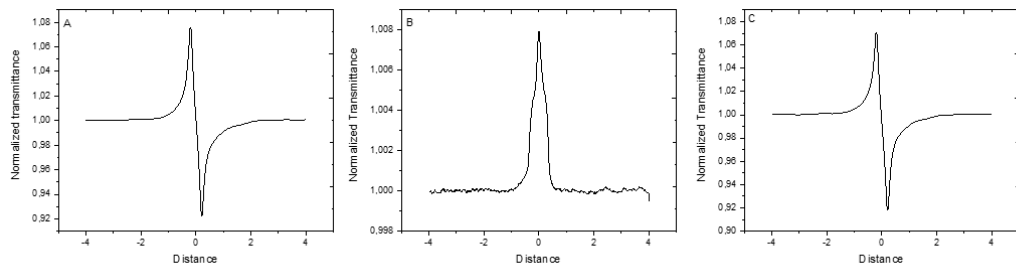


Figure 1.9 A) close aperture data B) open aperture data C) ratio, A/B

1.8 Theory of nonlinear refraction

In this part, nonlinear refraction phenomena will be discussed theoretically. Considering a Gaussian beam with the electric field $E(r,t,z)$ interacting with the matter, obtained data from Z-scan can be processed as follows (Figure 1.9); (i) In this step, $E(r,t,z)$ is described as a gaussian beam at a sample position z with respect to the focal point, $z=0$. (ii) a phase shift $\Delta\varphi(r,t,z,L)$ on the beam occur at the focal point due to the nonlinear refraction, (iii) then, gaussian beam will propagate to an aperture at a distance d from the focal point t , and (iv) lastly, the light intensity that passes through the aperture, $T(z)$, is recorded.

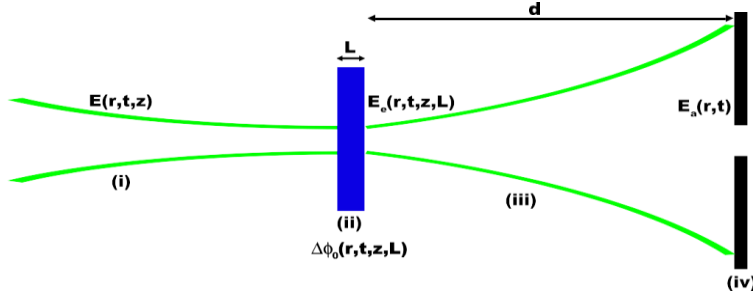


Figure 1.10 Propagation of gaussian beam along the z direction

1.8.1 Gaussian beam at the sample

Equation 1.9 presents a propagating electric field, $E(r, t, z)$ of a gaussian beam with a beam waist of w_0 along the z direction (Figure 1.9).²¹

$$E(r, t, z) = E_0(t) \cdot \frac{w_0}{w(z)} \cdot e^{\left(-\frac{r^2}{w^2(z)} - \frac{ikr^2}{2R(z)}\right)} e^{-i\varphi(z,t)} \quad 1.7$$

The beam radius, w does change along the z direction due to focusing and can be calculated by $w^2(z) = w_0^2 \left(1 + \frac{z^2}{z_0^2}\right)$. The curvature radius of the wavefront at z is given by $R(z) = z \left(1 + \left(1 + \frac{z^2}{z_0^2}\right)\right)$ here $z_0 = k \frac{w_0^2}{2}$ is known as Rayleigh range for the beam where $k = \frac{2\pi}{\lambda}$ is the wave vector and λ is the wavelength of the laser in free space.^[22-23]

1.8.2 Introducing the phase shift.

In Z-scan analysis, refractive index should be considered with both linear index of refraction and nonlinear index of refraction, n_2 (cm²/W) or γ (esu).^[24-25]

$$n = n_0 + \frac{n_2}{2} |E|^2 = n_0 + \gamma I = n_0 + \Delta n \quad 1.8$$

where n_0 is linear index of refraction, E is the electric field, and I is the intensity of the laser beam that propagates in the sample. Sample thickness is important for the

Z-scan analysis. Thickness of the sample that is investigated should be small enough for the change in beam diameter in sample because of diffraction or nonlinear refraction.

$$\frac{d\Delta\varphi(r,t,z,L)}{dz^t} = \Delta n(I)k \text{ and } \frac{dI}{dz^t} = -\alpha(I)k \quad 1.9$$

z^t is the propagation depth of a laser beam in the sample and $\alpha(I)$ includes terms for both nonlinear and linear absorption. Phase shift, $\Delta\varphi$ of the laser beam at the sample is written as

$$\Delta\varphi(r,t,z,L) = \Delta\varphi(t,z,L)e^{-\frac{2r}{w^2(z)}} \quad 1.10$$

$$\Delta\varphi(t,z,L) = \frac{\Delta\Phi_0(t,L)}{1+\frac{z^2}{z_0^2}} \quad 1.11$$

And on-axis phase shift at the waist, $\Phi_0(t)$, is defined as

$$\Phi_0(t) = k\Delta n(t)L_{eff} \quad 1.12$$

$$-L_{eff} = \frac{1-e^{-\alpha L}}{\alpha} \quad 1.13$$

$$\Delta n(t) = \gamma I_0(t) \quad 1.14$$

Here L is the sampling length (sample thickness), α is the linear absorption coefficient and can be obtained from the UV-VIS spectrum. $I_0(t)$ is the intensity of the laser beam at the focus ($z=0$). When phase shift due to passing through a sample is included then formula for the gaussian beam can be written as

$$E(r,t,z,L) = E(r,t,z)e^{\left(-\frac{\alpha L}{e^{i\Delta\varphi(r,t,z,L)}}\right)^2} \quad 1.15$$

Since L is a variable of the optical setup, parameter L can be omitted for the rest of the discussion. Therefore, formula can be written as

$$E(r,t,z) = E(r,t,z,L) \quad 1.16$$

1.8.3 Transmittance into aperture

Describing instantaneous transmittance through the sample as

$$Pi(t) = \frac{\pi w_0^2 I_0(t)}{2} \quad 1.17$$

$$S = 1 - \exp(-2r_a^2/w_a^2) \quad 1.18$$

is defined for the linear transmittance for the aperture where w_a is the radius of the beam at the aperture.²⁶ A significant parameter in Z-scan analysis is magnitude of S. Because large aperture size leads to decrease in variation $T(z)$. If the aperture size is too much, which corresponds to $S=1$, variation in the $T(z)$ would disappear and it becomes independent of position and phase change. Actually, this type of measurement is very close to nonlinear absorption coefficient measurement.²⁷

To simplified analysis, ΔT_{p-v} is measured, and it is value difference between normalized peak and valley transmittance. This numerical value can be calculated as a function of $|\Delta\Phi_0|$ and it has linear dependence with the aperture size. In addition to that, this value is independent of the geometry or laser beam wavelength. This relation can express as²⁸

$$\Delta T_{p-v} = 0.406(1 - S)^{0.25} |\Delta\Phi_0| \quad 1.19$$

This equation is very helpful to figure out nonlinear refraction value with good accuracy. Factors that affect this accuracy are setup design, calibration, and optical quality. Those factors may create errors greater than % 2. n_2 can be calculated by fitting the data to eq. 1.19²⁹. Nonlinear refractive index value can be extracted directly from fitting. Details are given in data analysis part of the next chapter.

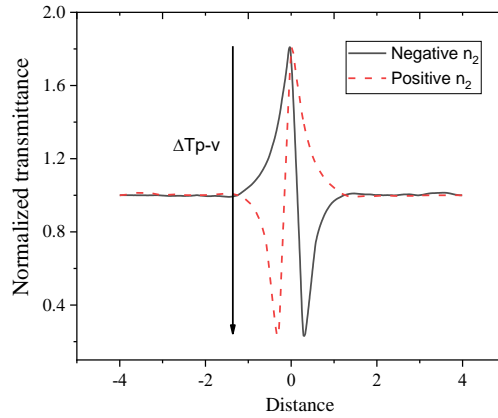


Figure 1.11 Representation of ΔT_{p-v}

1.8.4 Nonlinear absorption

As it was mentioned earlier, nonlinear absorption coefficient can be obtained with a Z-scan analysis. To measure it, aperture should be removed, and it makes the measurement insensitive of the nonlinear refraction.

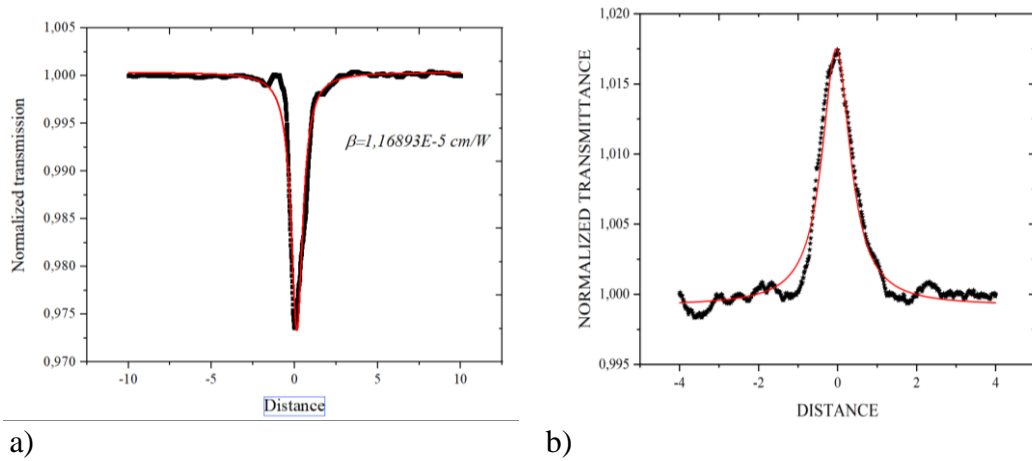


Figure 1.12 results of a) multi photon absorption, reverse saturable absorption, and b) saturable absorption.

Since gaussian beam intensity is symmetric around the focus, transmittance versus position graph should be symmetric. In addition to that, in those measurement transmittances can increase or decrease. While transmittance decreases in the multi photon absorption and reverse saturable absorption, transmittance increases in saturable absorption. Results of them are illustrated in Figure 1.11. Nonlinear absorption coefficient is extracted by fitting the data. Details are given in data analysis part of the next chapter.

1.8.5 Factors that affect the nonlinear optical properties

There are some factors that affects the nonlinear refractive index and nonlinear absorption coefficient values of the organic compounds. Firstly, the one factor that affects the nonlinear optical properties is conjugation of the interested organic compounds. Datta et al. studied the effects of conjugation length on the non-linear optical properties of organic push–pull compounds using density functional theory.³¹ They have reported that the best NLO properties were observed in organic compounds having pi-conjugated systems. Moreover, it has been indicated that, increase in the conjugation length leads to raise on the NLO response. Secondly, other factor is intermolecular charge transfer,^[32-33-34-35] and it has relation with the conjugation. An increase in the conjugation generally increases number of resonance structure. Because of that, it is expected to have an increased NLO respond.

Third factor is reported as HOMO-LUMO gap. It determines the hardness of the organic compounds.³⁶ Ali *et al* have reported the NLO properties of designed disubstituted quinoline with carbazole compounds. It has been stated that larger HOMO-LUMO gap increases the hardness^[37-38-39] and compounds which have hardness become resistive to charge transfer. This suggests that it would be harder to observe strong NLO behaviour on large ban-gap molecules.

Charge transfer is a key point on the nonlinear optical properties^[40-33] and charge transfer happens between donor and acceptor groups, especially for organic

compounds that have donor- π -acceptor (D- π -A) systems. A large number of studies in the literature report that increase in the donor ability of donor groups enhance the quality of the nonlinear response [41-42-43-44-45]. Therefore, during the examination of why a compound have good nonlinear response, consideration of the donor ability of the group would be another point to consider besides the HOMO-LUMO gap.

Aromaticity also has effect on nonlinear optical properties and strong correlation exists between the experimentally determined two photon absorption values and the presumed aromaticity⁴⁶. Aromatic molecules have high delocalization and stability. thus high nonlinear optical porperties⁴⁷.

CHAPTER 2

EXPERIMENTAL

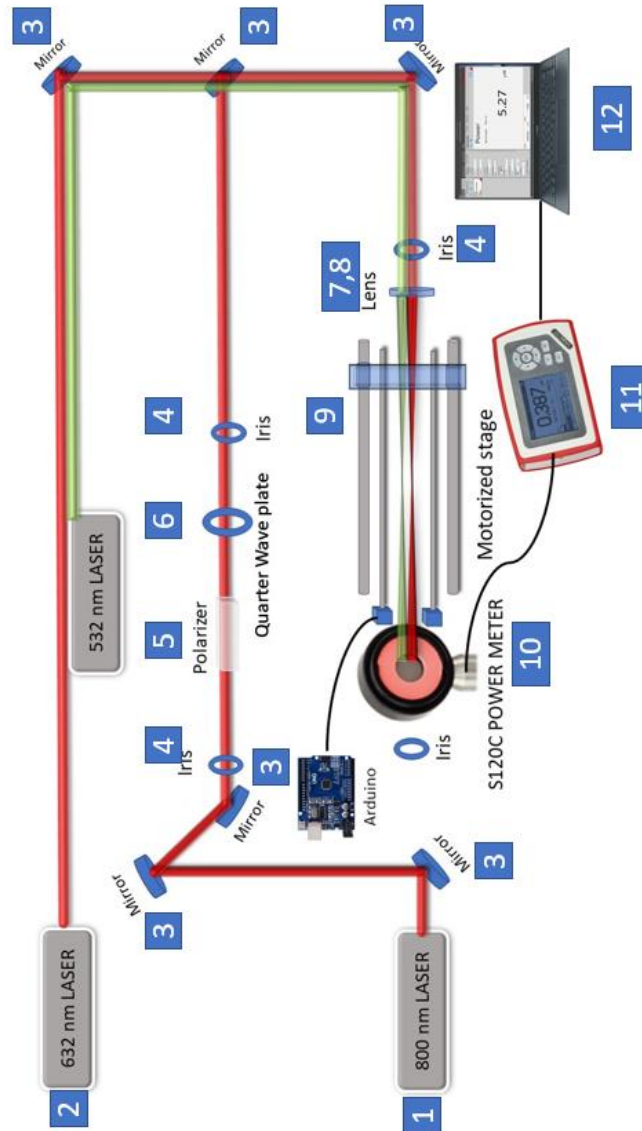


Figure 2.1 Z-Constructed final Z-scan setup

2.1 Z-SCAN system setup overview

Z-scan technique is becoming a widely applied technique to determine nonlinear optical properties of materials such as organic compounds⁴⁸ or 2D materials^[49-50-51]. With this aim, many trials were performed on the setup to obtain best performance and best result with the equipment at hand. The final version of the system was established with a 800 ultrafast Ti: Sapphire oscillator laser as a light source, and a 632.8 nm He-Ne laser light source. (Figure 2.2 and Figure 2.3) The power of the laser sources was measured by a power meter sensor and samples were translated with motorized stage. Equipment's of constructed system are listed at **Table 1**.

Table 1. The equipment of Z-scan system

Item	Item	Manufacturer	Model	Properties
1	Ti.Sapphire Mode-locked Laser	Coherent	Mantis-5	800 nm, 80 fs pulse duration, 80 nm pulse width, 80 MHz rep. rate, 550 mW output power
2	HeNe Laser	Melles Griot	25-LGP-193-230	632.8nm, 5mW
3	Dielectric mirrors (x6)	Thorlabs	BB1-E03	
4	Iris (x3)	Thorlabs	ID25	
5	Glan Thompson polarizer	Thorlabs	GTH10	
6	Quarter waveplate	Thorlabs	WPQ10M-808	Ø1/2" Mounted an RSP1D Continuous Rotation
7	Lenses, Plano-Convex Spherical	Thorlabs	LA1422-B	N-BK7, Ø1", f = 40.0 mm, ARC: 650-1050 nm

Table 2. The equipment of Z-scan system (Cont'd)

Item	Item	Manufacturer	Model	Properties
8	Lenses, Achromatic	Thorlabs	AC254- 100-B	Ø25.4 mm, f=100.0 mm, Near IR Achromat, ARC: 650 - 1050 nm
9	Motorized stage	Custom	Custom	Motorized stage with NEMA-17 stepper motor and Arduino Uno controller
10	Photodiode Power Sensor	Thorlabs	S120C	400 - 1100 nm, max measured power 50mW
11	Digital handheld optical power	Thorlabs	PM100D	100 pW to 200 W, 3 µJ to 15 J, 185 nm - 25 µm
12	Optical power monitor software	Thorlabs		Version 3.1

2.2 Main parts of the system with their properties

2.2.1 Lasers

An ultrafast Ti:sapphire oscillator laser that produce ultrashort pulses was used as light source (Figure 2.2). This laser has Titanium doped sapphire (Al_2O_3) with Ti^{3+} crystal that is pumped by 532nm and 5.5W green diode laser. Laser produces continuous wave (CW) and pulse radiation at 800 nm wavelength and around 600 mW power. Frequency of the pulse laser is 80 MHz In other words, laser generates 80 million pulses only in one second. By using this number of pulses, it is possible to calculate time between the pulses. If there is 80×10^6 pulses in a second,

time between pulses would be 12.5 ns ($=1/80 \times 10^6$). The pulses are ultrafast, and each pulse is only 100 fs long. That is why the laser is called an ultrafast system.



Figure 2.2 800nm laser source

Figure 2.3 shows the other laser source that is used in the setup. It produces continuous wave (CW) laser with wavelength of 632.8 nm, and its output is ca. 5 mW.



Figure 2.3 632.8 He-Ne laser source

2.2.2 Quarter waveplate and Glan Thompson polarizer

Quarter waveplate and Glan Thompson polarizer are used in the setup to adjust the amplitude of the 800 nm laser. (Figure 2.4) There are two reasons for that, one of the reasons is that measurable max laser power is 50 mW due to specs of the power sensor S120C. The other reason is that sometimes 50 mW or 30 mW are enough to burn the organic samples so laser power should be adjusted even 0-50 mW to protect the organic samples. Working principle of those two equipment is that quarter waveplate convert circularly polarized light into linearly polarized light. However, important point is which polarized light is obtained. It can be s or p polarized light. According to those polarization situation light can pass from the Glan Thompson polarizer. In this way amplitude can be adjustable.

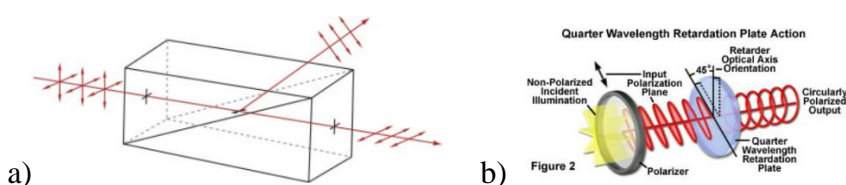


Figure 2.4 a) Glan Thompson polarizer b) working principle of quarter waveplate⁵²

2.2.3 Lenses

There are two different lenses are used in the setup. Those lenses are chosen to form the literature. Those are AC254-100-B and LA1422-B lenses. AC254-100-B achromatic lens have 10 cm focal length. Working interval of the lenses 650nm-1050nm. LA1422-B N-BK7 Plano convex lens has 4 cm focal length and working interval of the lenses is same as AC254-100-B achromatic lens

2.2.4 Motorized stage

In z-scan experiment, sample must be translated around the focal plane. Translating sample autonomously would be more practical.



Figure 2.5 Arduino Uno

Software controlled stage through an arduino uno (Figure 2.5) was established as in Figure 2.6. This motorized stage is controlled with the Nema 17 stepper motor. An arduino uno control unit was used to communicate with the controller. Arduino code for control the motor is written specifically for the setup. The start and end points of the stage was controlled with switches. The speed of scan across the focal plane can also be adjusted. This bring an advantages on the measurement time. A single measurement takes 15 or more min with a manual stage but it only takes 10 sec with a motorized stage. Breifly, thanks to motorize stage, setup is improved in terms of consumed time and data acquisition.

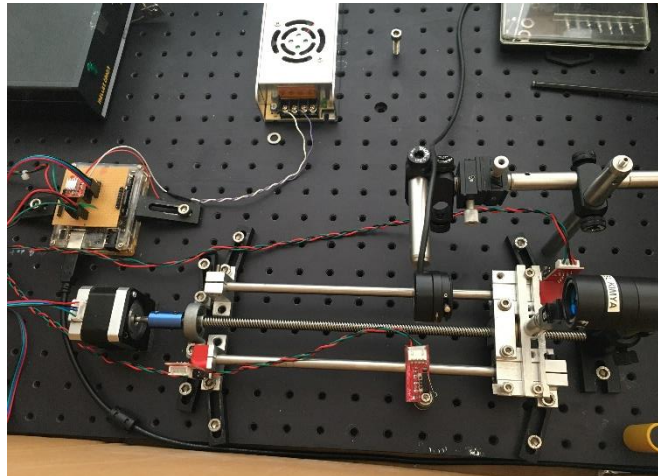


Figure 2.6 Motorized stage

2.2.5 Detectors

S120C - Standard Photodiode Power Sensor shown in Figure 2.8a is used in the optical setup. It is a Si sensor and has large area with an active detector area of 9.7 mm x 9.7 mm. It can detect 400-1100nm laser wavelengths, and its optical power range is 50 nW – 50 mW.

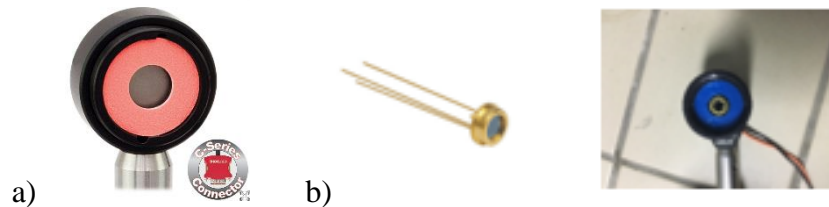


Figure 2.7 a) S120C Photodiode Power Sensor and b) FDS100-CAL - Calibrated Si detector

In our earlier versions of the optical set-up FDS100-CAL - Calibrated Si detector (Figure 2.8b) was used. Since its sensing area was too small, it was hard or impossible for many cases to collect all photons. Thus, this sensor needed to be very close to the focal plane where the beam size very small and made it hard to do a full scan. A larger detector enabled a longer scan range and capture of all the photons.

2.2.6 Data acquisition and analysis

In our earlier setup with FDS100-CAL detector data was recorded with Tektronix MS4101 oscilloscope shown in Figure 2.9

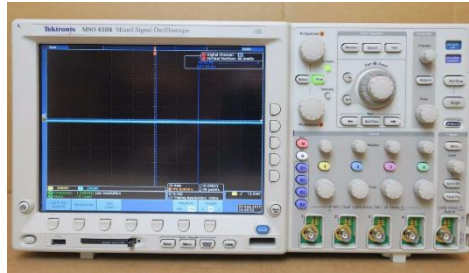


Figure 2.8 Tektronix MS4101

In the current setup, PM100D digital handheld optical power and energy meter shown in Figure 2.10 is used.



Figure 2.9 PM100D digital handheld optical power and energy meter

This power meter is connected to the computer with USB and data is collected via optical power monitor software that is shown in Figure 2.11 provided with Thorlabs Inc. In this software, power measurement can be performed with both the open aperture, and closed aperture setup.

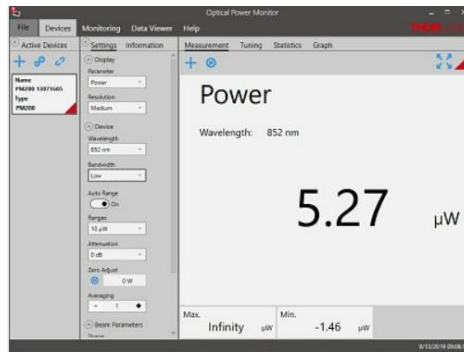
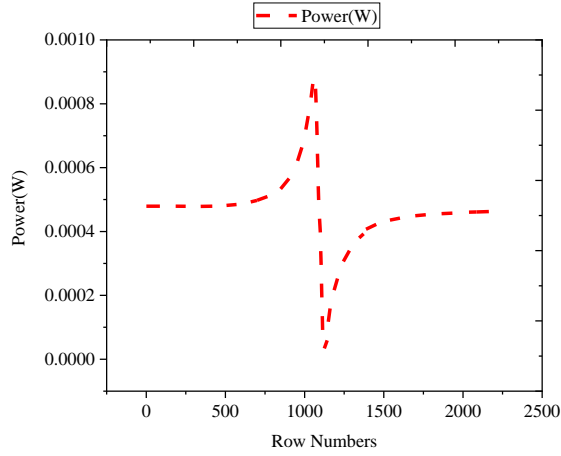
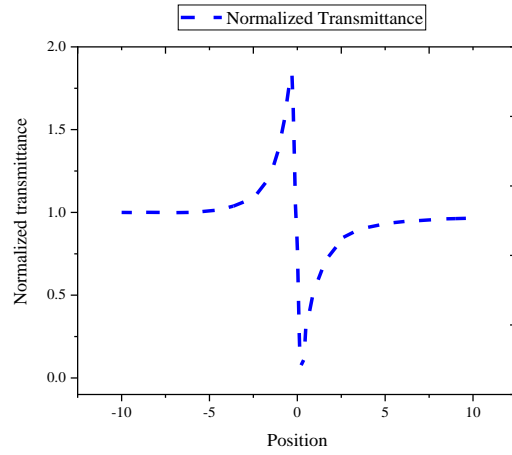


Figure 2.10 Optical power monitor software

The collected data are imported into a standard data processing software such as Excel or Originlab software. In the software normalization is performed by dividing all data to average of the first 10 data where no change in signal is observed to obtain normalized transmittance of the whole data. This way the power variation from measurement to measurement is eliminated. An example for a collected raw data and normalized data is shown Figure 2.13.



a)



b)

Figure 2.11 An example of a) a raw and b) normalized data

Once the normalized data is obtained, it was fitted to equations to extract nonlinear refractive index (n_2) and nonlinear absorption coefficient (β). Equations for the derivation of n_2 and β are as follows.

$$T(x) = 1 + \frac{4x\Delta\Phi}{(1+x^2)(9+x^2)} + \frac{4(3x^2-5)\Delta\Phi^2}{(1+x^2)^2(9+x^2)(25+x^2)} + \frac{32(3x^2-11)x\Delta\Phi^3}{(1+x^2)(9+x^2)(25+x^2)(49+x^2)} \quad 1.19$$

$$x = \frac{-z}{z_0} \quad 1.20$$

$$z_0 = \frac{\pi w_0^2}{\lambda} \quad 1.21$$

$$\Delta\Phi = kn_2 I_0 L_{eff} \quad 1.22$$

$$L_{eff} = \frac{1 - e^{-a_0 L}}{a_0} \quad 1.23$$

here, x refers to the positional point of the sample relative to the focal point ($z=0$). Z_0 is the Rayleigh range and $\Delta\Phi$ is the nonlinear phase shift at focus. The phase shift includes wavelength number (k), laser beam intensity at focus (I_0), and the effective sample thickness (L_{eff}). During extraction of nonlinear refractive index, equation 1.22 is substituted for the phase shift in equation 1.19.

$$T(z) = \sum_{m=0}^{\infty} \frac{\left[\frac{-\beta I_0 L_{eff}}{1 + \frac{z^2}{z_0^2}} \right]^m}{(m+1)^{3/2}} \quad 1.24$$

$$L_{eff} = (1 - e^{-a_0 L})/a_0 \quad 1.25$$

This fitting function is used to figure out nonlinear absorption coefficient (β) by fitting to the Normalized transmittance data.

Both fitting functions include sample thickness to find effective sample length. The sample thickness must be smaller than the Rayleigh length of the focused laser beam. This condition must be satisfied for correct observation of the nonlinear process.

Another important point is the background correction. Samples and cuvette that are used in the experiment can have linear responses or might be in poor quality. This situation can prevent to observe nonlinear effect due to the sample. It can be eliminated by performing two z -scan experiments. While the first experiment should be performed at the desired energy, the second experiment should be performed at the low energy.

The experiment that was performed with the low energy, become a background and it must be subtracted from the first data that was obtained from the first experiment.

When an experiment is performed in a solution the solvent effect must be considered.⁵³ To measure the effect of solvent, open and close aperture z-scan measurements of the pure solvent will be performed. Here, all conditions must be the same at which the experiment is performed for the sample.⁵⁴

2.2.7 Nonlinear refraction in cuvette material

Cuvette material may also have an effect on measurements. If the cuvette material has any nonlinear refractive index, closed aperture measurement should be performed and checked for the signal levels. If the nonlinear refractive index of the sample is much higher than the nonlinear refractive index of the cuvette material, it may be neglected.

2.2.8 Detector Area

Detector area is a factor that affects the measurements. When sample is translated around the focus point, all transmittance photons must be collected by the detector. In those measurements, SC120 power sensor is used. After a careful consideration of the possible positions of the detector, its position was adjusted such that all incoming photons are collected. However, during attempts, it was recognized that all photons cannot be collected by the sensor. It can be observed from the picture that is given in the below. There is a stray photon in the red shiny part of the sensor and this area is not the sensing area. Therefore, this type of measurements is generally wrong. To avoid from this situation, sensor should be moved closer to the lens.



Figure 2.12 Detector area

2.2.9 Sample preparation

For measurements either coated films or samples dissolved in solution were used. Since WS_2 has information about its nonlinear optical properties on literature, WS_2 was chosen as a reference substance. Unfortunately, WS_2 does not dissolve in solvents very well. Therefore, coating technique was used for measurements. All coatings were performed on microscope lame. Physical form of WS_2 is powder. In order to coat it is mixed with a volatile liquid like acetone or dichloromethane. All coating process was performed in home-made spin coater that is illustrated in Figure 2.13. However, it was creating homogeneity problem, so measurements were performed on lame parts that looks homogeneous and thickness was measured with a micrometer. For thickness measurement, two microscope lames were used. The first lame was used for coating and the other one was used for thickness measurement. Before coating, thickness of both lames was measured with micrometer. Finally, thickness of the WS_2 between two lames was measured. Generally, thickness was measured around $9\ \mu\text{m}$ and $11\ \mu\text{m}$. Organic compounds were dissolved in Dichloromethane in certain concentration and those compounds were measured with a quartz cuvette having 1 mm thickness.



Figure 2.13 Spin coating

2.2.10 Optimization studies

The most promising system was chosen, and then it was tuned for sample measurements. The final set-up parameters were examined and improved in this section of the study. These settings for the laser power, and stage speed.

2.2.10.1 Laser power

Intensity at the focus has important role for NLO response. Because if the laser intensity increases NLO response increase. However, one needs to be also careful on the laser power since compounds that are measured should not be damaged at focus point. In other words, compounds should not be burnt due to high intense laser beam at focus. Therefore, laser power should be chosen carefully. Therefore, measurements were performed from low laser power to threshold power. In addition to that, measured compound cannot show any NLO responses at low laser power. For WS₂, laser power adjustment was performed, and optimum laser power is determined as 40mW. Results are given in Figure 2.15

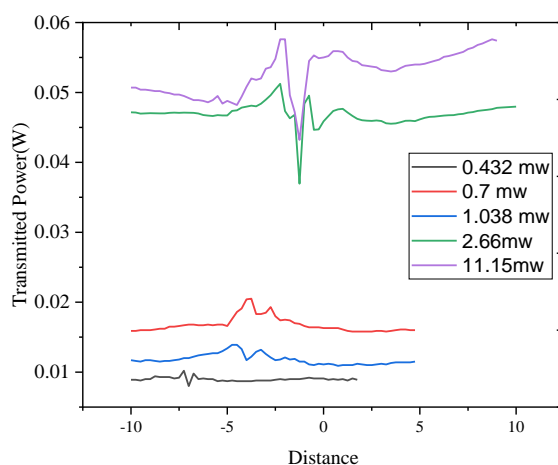
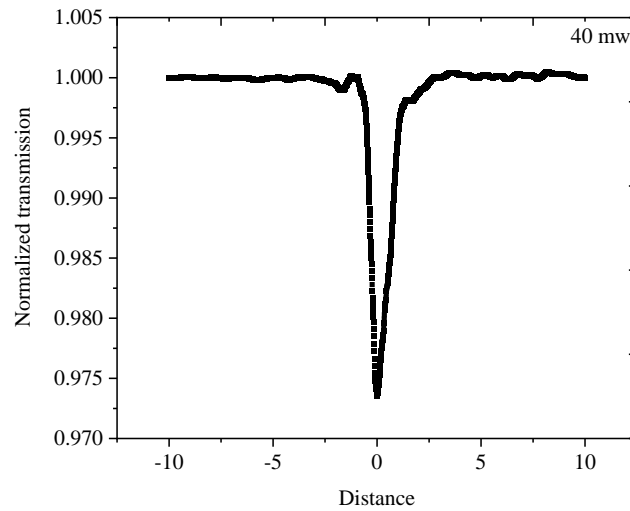
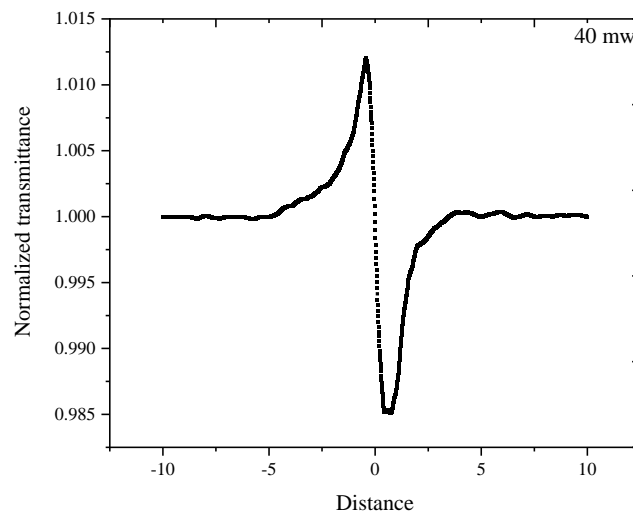


Figure 2.14 WS₂ measurements in different laser power.

In Figure 2.14, data looks like noisy due to the signal to noise ratio and clear NLO response are not observed at this power level. However, when laser power is increased from this level to 40 mW a strong NLO response that is illustrated in Figure 2.15 is observed.



a)



b)

Figure 2.15 An example of strong a) nonlinear absorption and b) nonlinear refractive index response of WS_2 at 40 mW

2.2.10.2 Stage speed

Arduino controlled motorized stage was used to translate sample around focal point. In our initial work, translation is done with manual stage. Here, sample translation and data capturing were also performed manually. Manual operation of the micrometer stage and the software makes the data collection very slow and time consuming. Data collection takes around 45 min with manual stage for 25 data point collected. By establishing motorized stage, time for collecting data is decreased from 45 min to 15 sec and number of data points is increased from 25 to 1000 data points. Speed of motorize stage can be adjusted with Arduino code written specifically for this system. During translation, data was captured via power meter sensor and Thorlabs software. The speed of the translation stage is adjusted with careful considerations and experimental observations of the sensor sensitivity to make sure the correct data collection. In high translation speed, sensor is not fast enough to capture the data at the point and either misses the data or results in spread of the data over many points. The correct data is obtained with step scan and making sure the signal levels at the positions. Then the continuous scan data is compared to those. The scan speed is carefully chosen as the fastest speed of scan possible without losing any information from the original data. Figure 2.16 represents a successfully collected data.

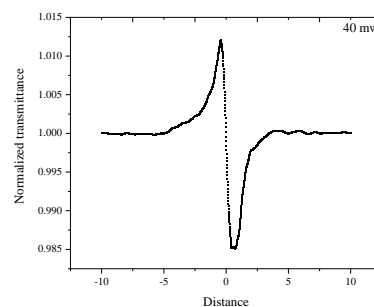


Figure 2.16 An example of successfully collected data.

2.2.10.3 Repeatability studies

During repeatability measurement, 5 repeated scans of the same compounds were performed with our constructed Z-scan setup. 2 of the scans were performed by using the same solution but moving the quartz cuvette out and then into the sample position back again and 3 of the scans were performed by refilling quartz cuvette with the same solution of the compound. After 5 measurements were performed, averaging was applied on data of 5 scanning and standard deviation is calculated. For example, in one of the measurement the mean is 6.30×10^{-7} and the error is $\pm 0.05 \times 10^{-7} \text{ cm}^2/\text{W}$ for the nonlinear refractive index. Measurements with error bars that is illustrated with red colour are given in Figure 2.17. The error is less than 1%.

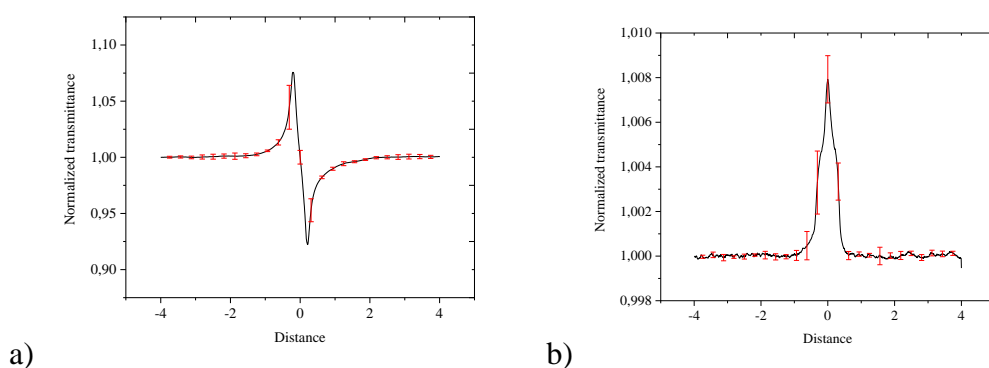


Figure 2.17 Example of a) closed aperture measurement and b) open aperture measurement with error bars.

2.2.11 Experiences from past to present on constructed setup.

Here, I will write a short story of my experiences on the Z-scan setup construction. Firstly, 800 nm laser fs pulsed coherent Mantis-5 was used as laser source. Setup was located on optical table and given in Figure 2.17.

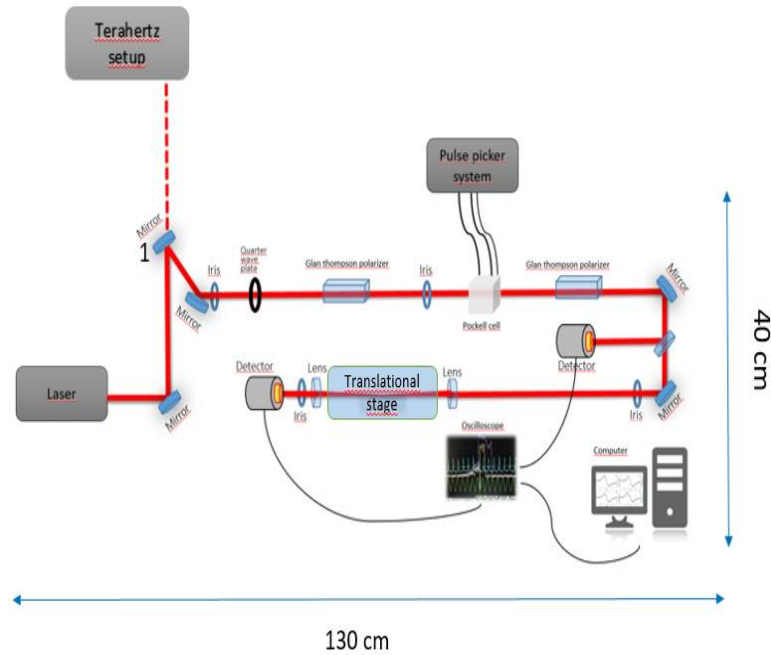


Figure 2.18 First constructed setup

In this setup, Pulse Picker system to decrease the laser pulse number per second, polarizer, quarterwave plate, pockel cell, FDS100-CAL - Calibrated Si detectors produced by Thorlabs, manual stage, 5 mirrors, 4 irises, and 2 lenses, Tektronix MSO 4104 was used. Reason for the usage of Pulse picker system is that detector become saturated when exposed with 80 MHz laser pulses. Therefore, 80 MHz was reduced to 1KHz with the Pulse Picker system. Here, working principle of pockel cell and Pulse Picker system should be explained. The Glan Thompson (GT) polarizers are providing selectivity on s and p polarization. Here, the first one cleans the laser beam and provides only p polarization to the Pockels cell. This is required polarization for the operation of the Pockels cell. The second GT polarizer only passes polarized light if the polarization is rotated with the help of the Pockels cell operation. Otherwise,

no light exits through the Pockels cell The Pockels cell only rotates the polarization under applied high voltage. In Figure 2.18, working principle of Pockels cell is shown.

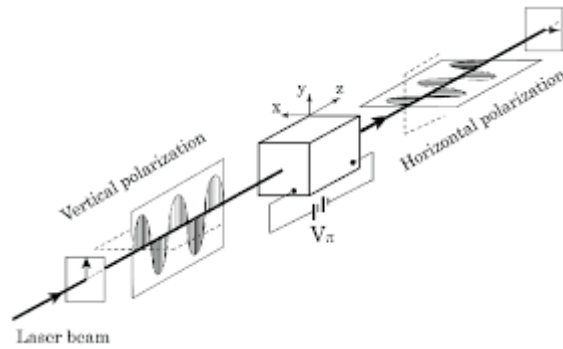


Figure 2.19 working principle of Pockels.

A schematic representation of working principle of Pulse picker system is shown in Figure 2.19. The high voltage is provided by this system. It can provide a high voltage between 5 and 6 kV. There are two channels that carry the turn-on and turn-off TTL signals to the controller above the Pockels cell in times received by those signals. In our setup this time is very close to 12.5 ns that is the time between two pulses. Therefore, we sometimes collect one or two pulses depending on the settings. Figure 2.19 shows the simulated laser pulses and overlapping TTL pulses to turn HV on and off on the Pockels cell that can extract a single laser pulse once the Pockels cell operates.

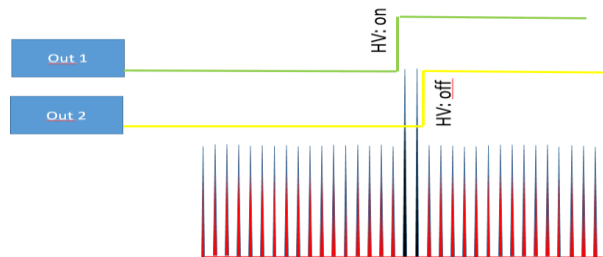


Figure 2.20 Schematic drawing of working principle of pulse picker system

With this way, the system was made ready for data collection that is illustrated in Figure 2.20

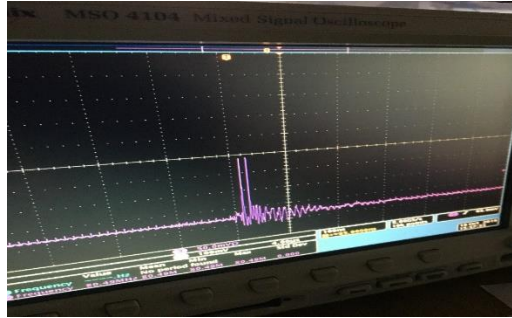


Figure 2.21 Collected two pulse in our system.

After study about data collection, manual stage (Figure 2.21) was established to translate sample from lens to detector.



Figure 2.22 Manual stage

However, manual stage brings disadvantages that is explained in the stage speed part in optimization stage. In Figure 2.22, nonlinear refractive index measurement is illustrated and there are 25 data point in measurements. In final setup, 25 data point was increased 1000 data point with motorized stage.

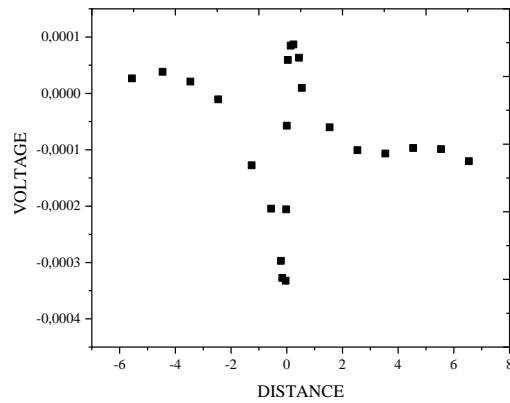


Figure 2.23 nonlinear refractive index measurement with manual stage.

In first trail of setup, detector area of FDS100-CAL become important in measurement. During measurement, it was realized that not all photons can be measured by the detector. Therefore, signal alteration that is measured by detector cannot be obtained completely, in order to solve this problem, a lens was used to focus beam on detector that is shown in Figure 2.23 and data that was obtained with this configuration is given in Figure 2.24



Figure 2.24 Lenses, manual stage, and detector.

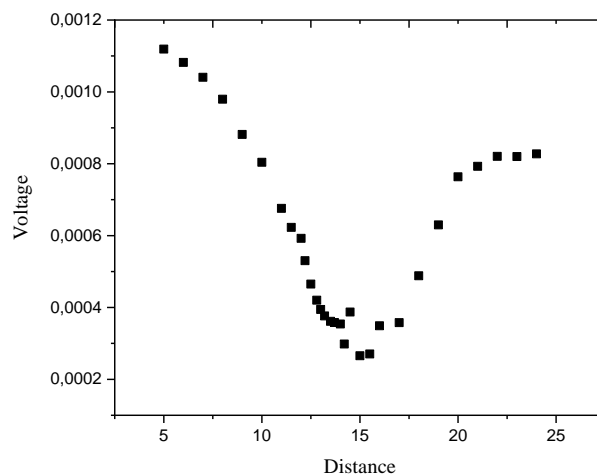


Figure 2.25 Collected data with lenses that is located in front of detector

Measurements continued to be taken with this configuration for a while. However, this configuration was abandoned due to insufficient results mainly due to small scanning range. After all those processes, power meter sensor was used as a last decision. It has large detector area, and it is more sensitive than FDS100-CAL detector. In this way, detector area problem was solved. Thanks to power meter sensor, pulse picker system and pockell cell were not used in current setup, because its sensitivity is enough for photon measurement. After that, motorized stage was established and integrated in setup and proper data were collected and those data were illustrated in verification of setup part. In addition to that, 632.8m nm He-Ne laser was integrated in laser path. Finally, the last setup (Figure 2.1) was constructed, and organic compounds were measured and results of them presented and discussed in result and discussion part.

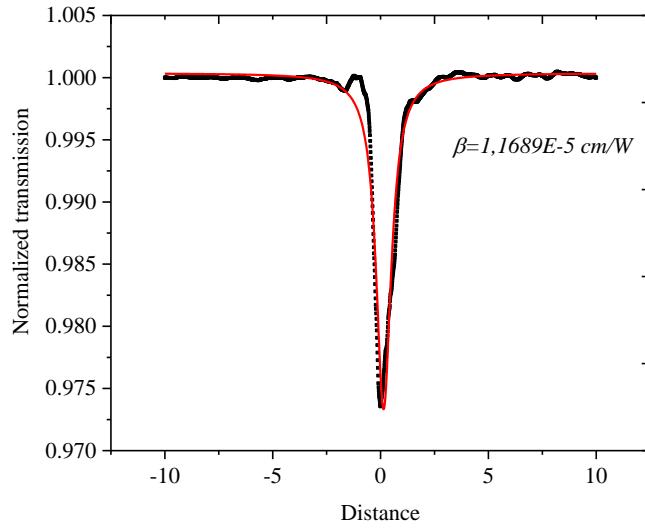
CHAPTER 3

RESULT and DISCUSSION

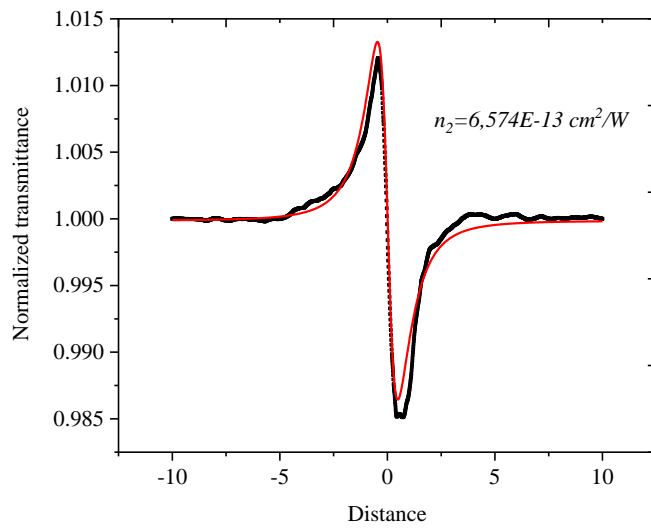
3.1 Verification of constructed setup with literature

Z-scan optical setup once was constructed, the aim is now the investigation of nonlinear optical properties of unknown organic compounds. However, the system needs to be tested. In order to test and verify the correctness of the data collected by the optical system, the data collection and processing of two nonlinear materials with known nonlinear optical properties were chosen from the literature: tungsten disulfide (WS_2) and methylene blue.

The first reference sample was WS_2 . Zheng *et al* has reported the nonlinear refractive index for the WS_2 monolayer⁵⁰. In this work, 800 nm laser and 10 cm focal length lens were used. In addition to that, different intensities have been investigated. They claim that as the power density is increased transition between saturable absorption and reverse saturable absorption has been observed. They have reported the nonlinear refractive index and nonlinear absorption coefficient as 8.1×10^{-13} m/W, and 3.7×10^{-6} m/W, respectively. In our measurements, nonlinear refractive index value has been obtained as 6×10^{-13} m²/W, nonlinear absorption coefficient has been calculated as 1.1×10^{-5} m/W. Both the nonlinear index and absorption coefficients are in similar order of magnitude. The difference possibly is from the sample variation where they have deposited the sample while we have filmed on glass. Max usable laser power before burning the sample is 50mW. In other words, intensity at focus point must be below the 275 GW/cm². In the article, saturable absorption is observed below at this intensity. It is reason why increasing in transmittance in focus is observed. it is again strong evidence in terms of trustworthy of constructed setup. After experimental values for nonlinear refractive index and nonlinear absorption coefficient of WS_2 were figured out, experimental system parameters are extracted from the data.



a)



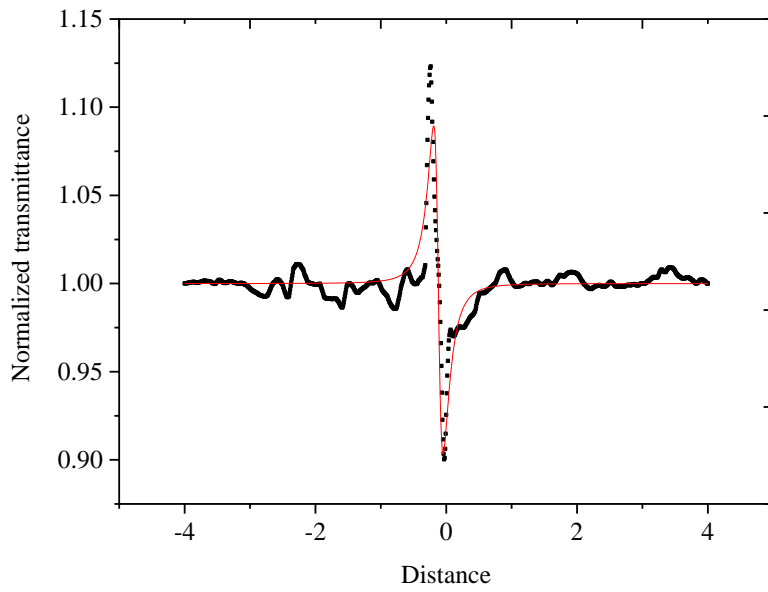
b)

Figure 3.1 Experimental for a) nonlinear refractive index and b) nonlinear absorption coefficient of WS₂ films.

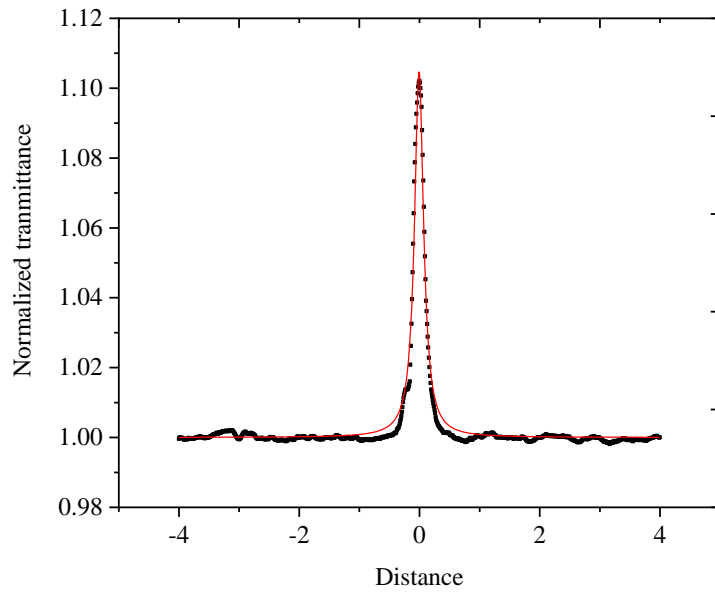
Table 3 Extracted setup parameter

Parameter name	Parameter value	Unit
Wavelength	800	nm
Laser power	500	mW
Focal length of laser	10	cm
Scan Length	20	cm
Spot diameter	27	μm
Beam intensity at focus	2780	W/cm^2

Open and closed aperture data of the methylene blue was collected as second reference sample and the nonlinear refractive index and nonlinear absorption coefficient from the measurements were extracted. Measurements were done with 632.8nm laser wavelength, 5 mW laser power, and lens with 4cm focal length. Figure 3.1 presents the closed and open aperture measurements of methylene blue.



a)



b)

Figure 3.2 a) Close and b) open aperture measurements of MB

We have compared the nonlinear properties determined with our setup with the results from the literature. In a study of Jeyara et. al. nonlinear absorption coefficient and nonlinear refractive index of methylene blue at three different concentrations were investigated.⁵⁵ In this work, 632.8 nm He-Ne laser beam with 5mW and a lens with 5 cm focal length were used. In their study they have performed both the open and closed aperture measurements and reported nonlinear refractive index and nonlinear absorption coefficients. Table 4 compares the NLO of methylene blue determined with our set-up to the literature. Our results are not only in similar order of magnitudes but also very close, especially of nonlinear refractive index. Differences may arise from the slight variation in concentrations.

Table 4. Nonlinear refractive index and absorption coefficient of methylene blue.

Dye concentration (mM)	$n_2 \times 10^{-7}$ (cm^2/W)	$\beta \times 10^{-2}$ (cm/W)	
0.05	-9.17	-2.58	Ref [24]
0.05	-8	-0.6	exp.

After experimental values for nonlinear refractive index and nonlinear absorption coefficient of methylene blue were determined, experimental system parameters were also extracted. (Table 5) Those parameters are spot diameter and beam intensity. system parameters were difficult measure thus determined experimentally and were used in measurements of unknown sample. The spot diameter is close to the one determined from WS₂.

Table 5. Extracted setup parameter along with the setup parameters of the instrument used for data collection.

Parameter name	Parameter value	Unit
Wavelength	632.8	nm
Laser power	5	mW
Focal length of laser	4	cm
Scan Length	8	cm
Spot diameter	30	um
Beam intensity at focus	289	W/cm^2

Now that the instrument is tested and verified, and experimental values for nonlinear refractive index and nonlinear absorption coefficient of methylene blue was determined successfully, two experimental parameters of the instrument were extracted from the fitting function. Those parameters are spot diameter and beam intensity. Those parameters can be measured with the beam profiler, unfortunately we do not have one. Therefore, extracting those parameters from the fitting functions is the best practical way to do it for our setup. This is a better and more accurate way than estimating the parameter values from the laser power and the focusing lens, then they are being used in measurements of unknown sample.

3.2 Introduction of organic push-pull compounds

The nonlinear response of organic compounds due to large nonlinear optical susceptibility properties has gotten recently significant attention in scientific community.⁴⁸ Organic compounds can have by design strong conjugation and tunability associated with acceptor and donor properties by adjusting the groups. This brings a possibility in tuning its nonlinear optical behavior. Therefore, investigation of the origin on nonlinear optical properties of organic compounds become significant question to pursue an answer. In this study, we will use the newly constructed Z-scan setup for the analysis of the nonlinear properties of a series of

organic compounds that vary in their donor group and acceptor group to observe the both the donor effect and the acceptor effects on the nonlinear properties. The series of compounds were provided by Çağatay Dengiz research group. Details of their synthesis mechanism and the characterization can be found in Reference⁵⁶.

3.3 HOMO-LUMO gap of TCNQ and TCNE based compounds

Theoretical calculation of highest occupied molecular orbital (HOMO) – lowest unoccupied molecular orbital (LUMO) values for those samples has been performed by Dengiz et al.⁵² HOMO-LUMO gaps are one of the important parameters for intermolecular charge transfers. In Table 6, location of the HOMO and LUMO in the structures is shown and electrostatic potential map is given. In all structures, they observed that while diethyl aniline group is the region of the HOMO, cyano groups (center structure) is the region of the LUMO. It means that charge transfer takes place from the donor groups to acceptor groups. In addition, electrostatic potential map (ESP) is helpful to figure out total charge density. When red and blue color are observed, blue color represents the diethyl aniline groups, which is the donor groups and red color represents the cyano groups, which is the acceptor group.

Table 6 HOMO-LUMO and ESP map. Reprinted from [52] with permission

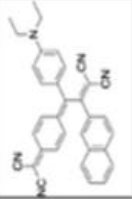
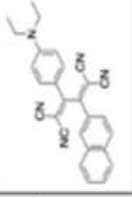
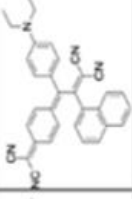
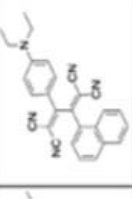
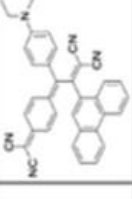
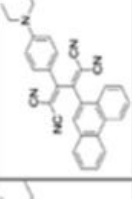
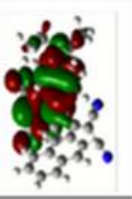
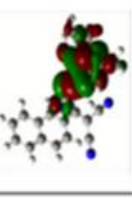
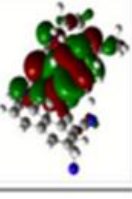
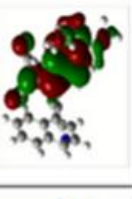
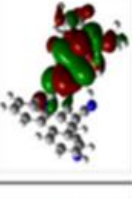
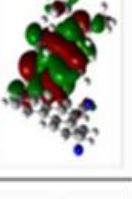
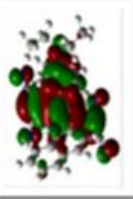
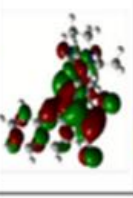
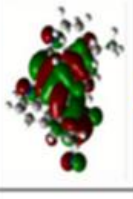
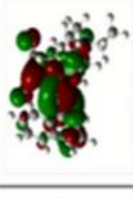
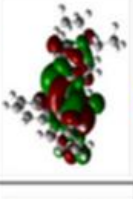

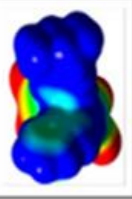
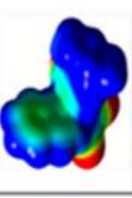
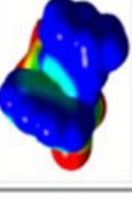
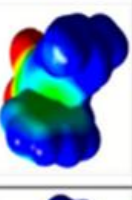
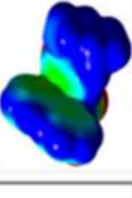
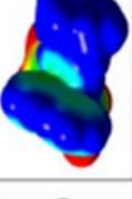
	Compound 3.2	Compound 3.1	Compound 2.1	Compound 2.2	Compound 1.1	Compound 1.2
Molecular Structure						
HOMO						
LUMO						
ESP						

Table 7 HOMO-LUMO gap for the compounds

TCNQ based compounds		TCNE based compounds	
Compound 1.1	1.73 eV	Compound 1.2	2.28 eV
Compound 2.1	1.72 eV	Compound 2.2	2.30 eV
Compound 3.1	1.87 eV	Compound 3.2	2.57 eV

In, Table 7 HOMO-LUMO gaps for the compound are given. When calculated HOMO-LUMO gap is investigated, it is obvious that there is a distinction between TCNQ based, compounds (1.1,2.1,3.1), and TCNE based, compounds (1.2, 2.2,3.2). Since electrons transfer occurs between HOMO-LUMO levels, this distinction affects the amount of charge transfer among sample. Small HOMO-LUMO gap generally means strong nonlinear optical response due to the high charge transfer, possibly due to large polarization formation.

3.4 Sample Preparation and UV-VIS spectra of the compounds

A correct sample preparation is an important step for good data collection. These organic compounds are soluble in DCM, thus we have prepared various concentrations of the samples for investigation. We have obtained good results with 0.2 mM solution in DCM. In order to extract the effective sample thickness and later the nonlinear absorption coefficient, their linear absorption coefficient at the laser wavelength is needed. Therefore, UV-VIS spectra of each solution were measured. The linear absorption coefficient is extracted from Beer's law as follow:

$$A = \varepsilon * b * c \quad 1.26$$

$$A = a * b \quad 1.27$$

Here A is absorbance, ε is molar absorptivity, c is the concentration and a is the linear absorption coefficient corresponding to $\varepsilon*c$. After, extraction of the linear absorption coefficient, effective sample thickness can be calculated with eq 1.29 in unit of cm or mm.

$$L_{\text{eff}} = \frac{1 - e^{-aL}}{a}$$

1. 28

UV-VIS spectra of those organic compound are presented in Figure 3.7

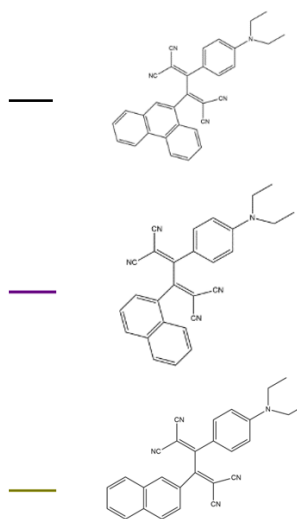
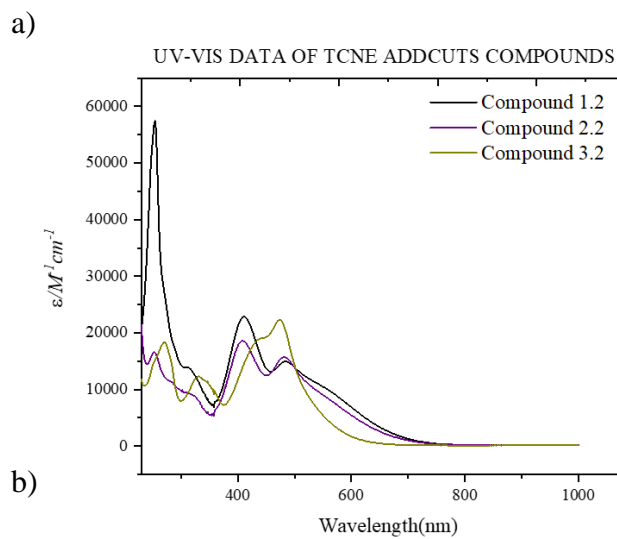
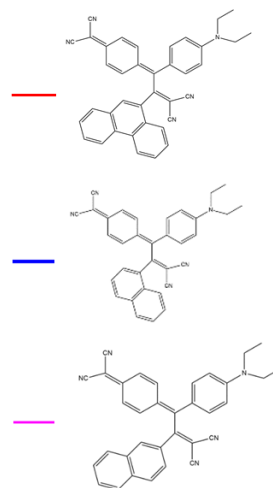
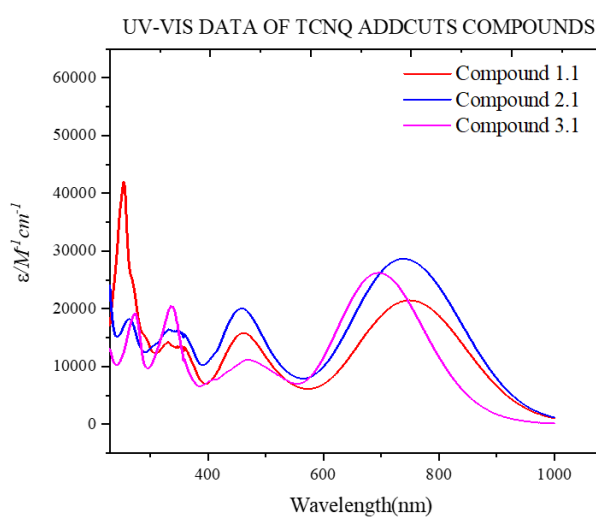


Figure 3.3 UV-VIS spectrum of a) TCNQ and b) TCNE with alkynes substituted by electron-rich diethyl aniline and polycyclic aromatic hydrocarbons compounds.

3.5 Z-scan measurements of TCNE and TCNQ with alkynes substituted by electron-rich diethyl aniline and polycyclic aromatic hydrocarbon

3.5.1 Compound 1.1

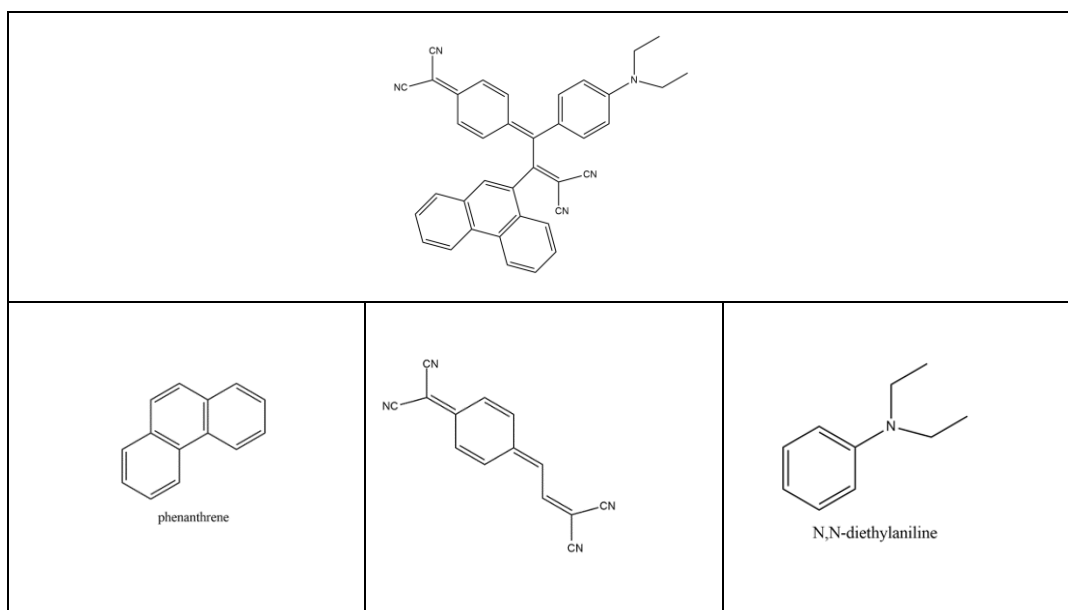


Figure 3.4 Molecular structure and fragmentation of compound 1.1.

Compound 1.1 consists of diethyl aniline and phenanthrene as polycyclic aromatic ring and those groups connects to the polycyno unit. It is a TCNQ based compound and its physical structure is powder, and its color is dark green. In UV-VIS spectrum, Compound 1.1 has molar absorption coefficient ϵ of $18820 M^{-1}cm^{-1}$ at 800nm and of $9966 M^{-1}cm^{-1}$ at 632nm. In addition to that, in UV-VIS spectrum of the Compound 1.1, it has absorption both 632.8 nm and 800 nm. However, it is more proper candidate for the 800 nm laser. Therefore, 0.2 mM dissolved compound 1.1 in DCM was measured under 800 nm pulsed laser with 40mW laser power and 632.8 nm He-Ne laser with 5.7 mW laser power. Normalized transmission profiles of closed and open aperture Z-scan measurements results for the Compound 1.1 at both 632.8 nm and 800 nm are given in the Figure 3.6 and 3.7

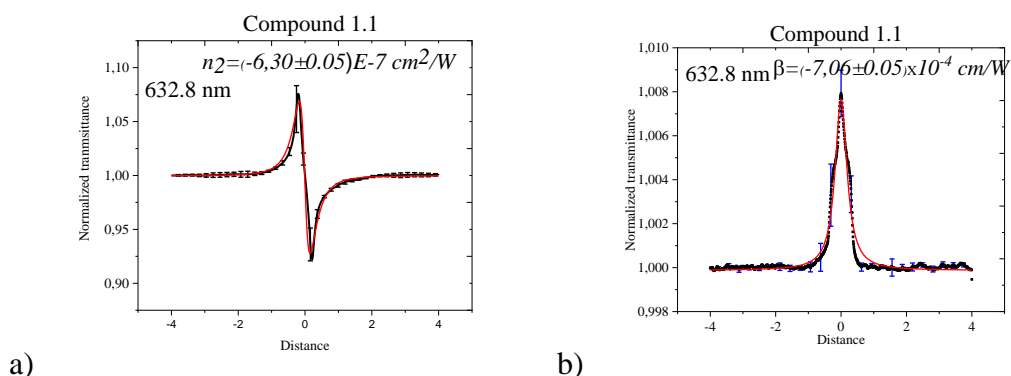


Figure 3.5 a) Closed and b) open aperture Z-scan measurement results of 0.2 mM compound 1.1 in DCM at 632.8 nm.

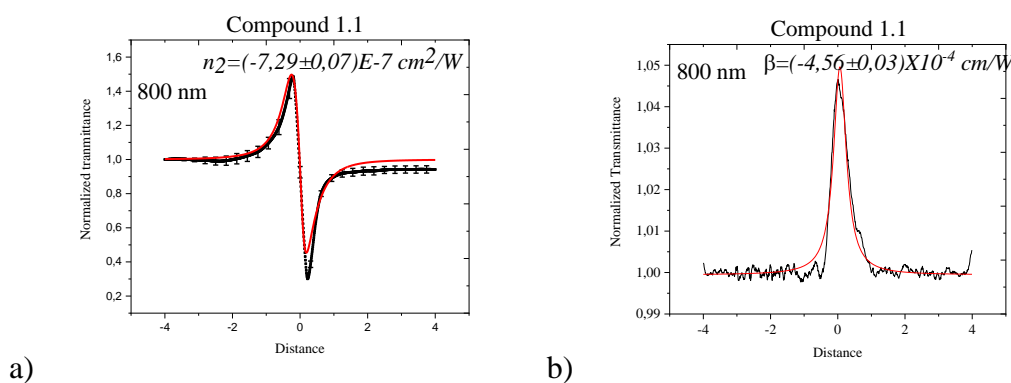


Figure 3.6 a) Closed and b) open aperture Z-scan measurement results of 0.2 mM compound 1.1 in DCM at 800 nm.

When 800 nm and 632.8 nm Z-scan measurement were compared, nonlinear refractive index n_2 and nonlinear absorption coefficient β of compound 1.1 is figured out as $(-6.30 \pm 0.05) \times 10^{-7} \text{ cm}^2/\text{W}$ and $(-7.06 \pm 0.05) \times 10^{-4} \text{ cm/W}$ for 632.8 nm, respectively, and $(-7.29 \pm 0.07) \times 10^{-7} \text{ cm}^2/\text{W}$ and $(-4.56 \pm 0.03) \times 10^{-4} \text{ cm/W}$ for 800 nm, respectively. It is noticed that measurement with 800 nm laser is resulted a stronger response. Maybe it can be related with the intensity of the laser beam because 5.7 mW is the max power of the 632.8 nm laser and beam power was 40 mW for the 800 nm laser. In Compound 1.1, charge transfer is occurred between diethyl aniline and polycyno group and it has long conjugation path due to the

phenanthrene and other aromatic ring. Therefore, it is expected that Compound 1.1 has strong NLO properties.

3.5.2 Compound 1.2

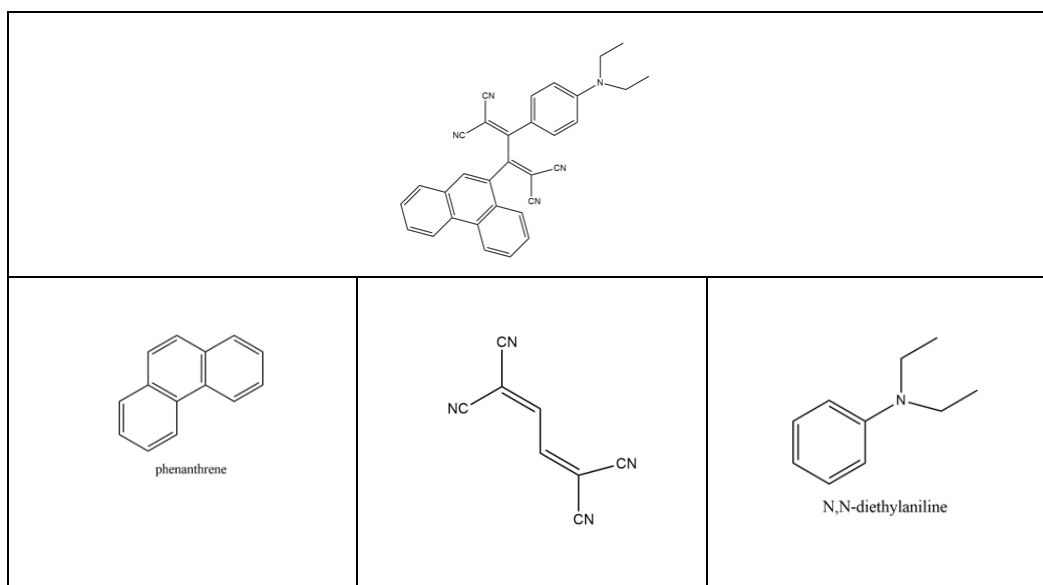


Figure 3.7 Molecular structure and fragmentation of compound 1.2

Compound 1.2 consists of diethyl aniline and phenanthrene as polycyclic aromatic ring and those groups connects to the polycyno units. It is a TCNE based compound and its physical structure is solid, and its color is dark purple. In UV-VIS spectrum, Compound 1.2 has molar absorption coefficient of $4460 \text{ M}^{-1}\text{cm}^{-1}$ at 632.8 nm and $147.03 \text{ M}^{-1}\text{cm}^{-1}$ at 800 nm. Nonlinear properties of the compound 1.2 were investigated by its 0.2 mM solution in DCM. The measurements were done at 800 nm with 26 mW laser power and at 632.8 nm He-Ne laser with 5.7 mW laser power. Normalized transmission profiles of closed and open aperture Z-scan measurements for the Compound 1.2 at both 632.8 nm and 800 nm are given in the 3.9 and 3.10.

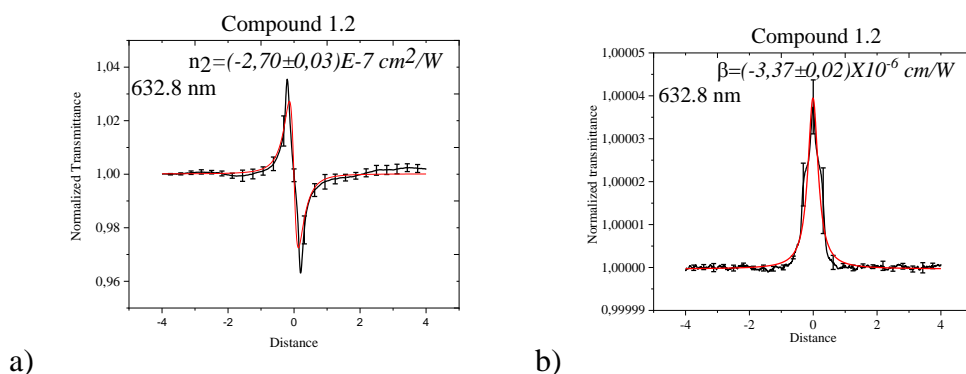


Figure 3.8 a) Closed and b) open aperture Z-scan measurement results of 0.2 mM compound 1.2 in DCM at 632.8nm

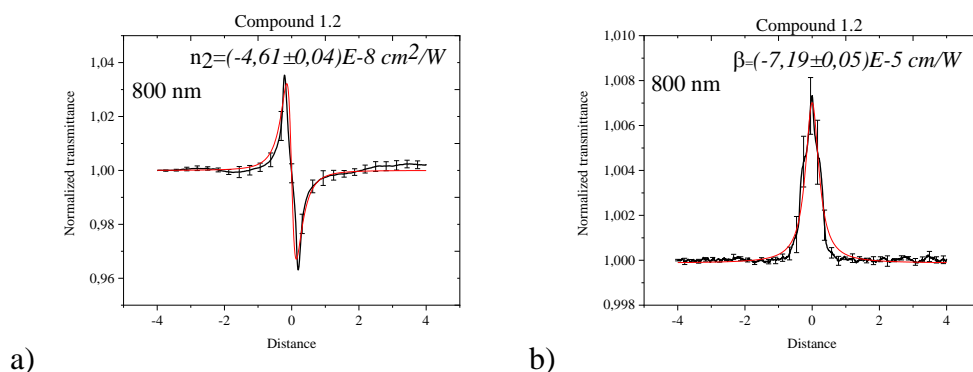


Figure 3.9 a) Closed and b) open aperture Z-scan measurement results of 0.2 mM compound 1.2 in DCM at 800 nm

When 800 nm and 632.8 nm Z-scan measurement were compared, nonlinear refractive index n_2 and nonlinear absorption coefficient β of compound 1.2 is figured out as $(-2.70 \pm 0.03) \times 10^{-7} \text{ cm}^2/\text{W}$ and $(-3.37 \pm 0.02) \times 10^{-6} \text{ cm/W}$ for 632.8 nm measurements, respectively, and $(-4.61 \pm 0.04) \times 10^{-8} \text{ cm}^2/\text{W}$ and $(-7.19 \pm 0.05) \times 10^{-4} \text{ cm/W}$ for 800 nm measurements, respectively. In Compound 1.2, charge transfer occurs between dimethyl aniline and polycyno group. However, when it is compared with the Compound 1.1 only difference is that Compound 1.2 has TCNE structure in it. Here, one aromatic ring is omitted from the structure, and it leads to shortening on the conjugation path, hence an increase in HOMO-LUMO gap. So nonlinear refractive index and nonlinear absorption coefficient value is expected to be less than

Compound 1.1. Experimentally, Compound 1.2 showed lower nonlinear refractive index and nonlinear absorption coefficient values than that of the Compound 1.1.

3.5.3 Compound 2.1

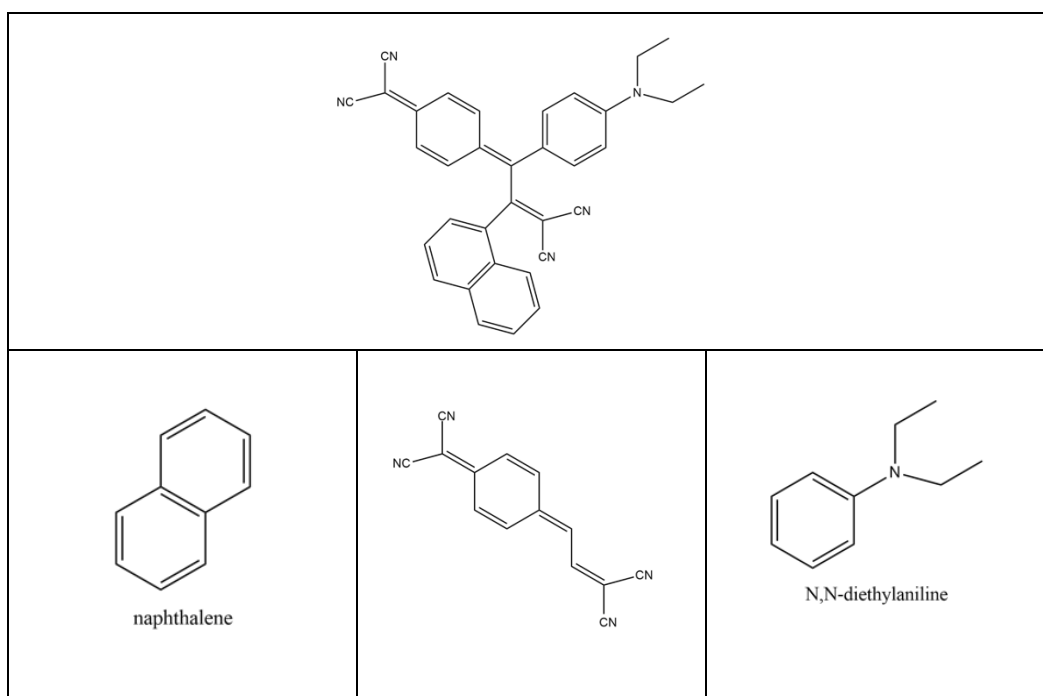


Figure 3.10 molecular fragmentation of compound 2.1

Compound 2.1 consists of diethyl aniline and naphthalene as polycyclic aromatic ring and those groups connected to the polycyno units. Its physical structure is powder, and its color is dark green. In UV-VIS spectrum, Compound 2.1 has molar absorption coefficient is $23839 M^{-1}cm^{-1}$ at 800 nm and is $14762 M^{-1}cm^{-1}$ at 632.8 nm. 0.2 mM Compound 2.1 dissolved in DCM was measured under 800 nm pulsed laser with 26mW laser power and 632.8 nm He-Ne laser with 6 mW laser power. Normalized transmission profiles of closed and open aperture Z-scan measurements for the Compound 2.1 at both 632.8 nm and 800 nm are given in Figure 3.12 and 3.13.

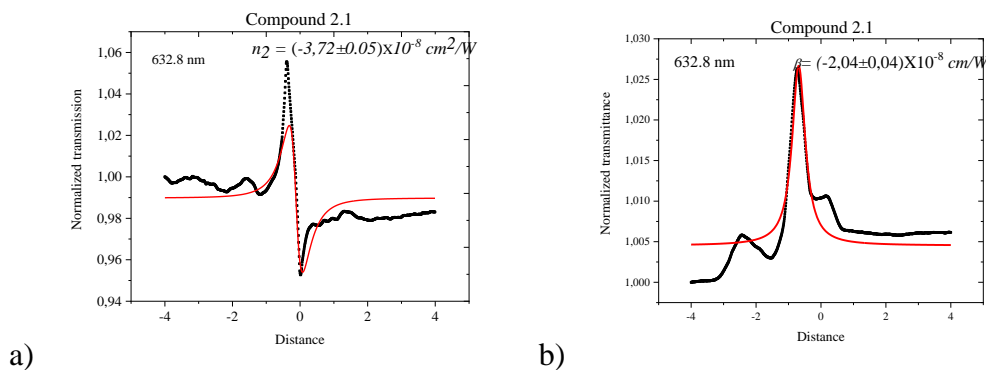


Figure 3.11 a) Closed and b) open aperture Z-scan measurement results of 0.2 mM compound 2.1 in DCM at 632.8 nm.

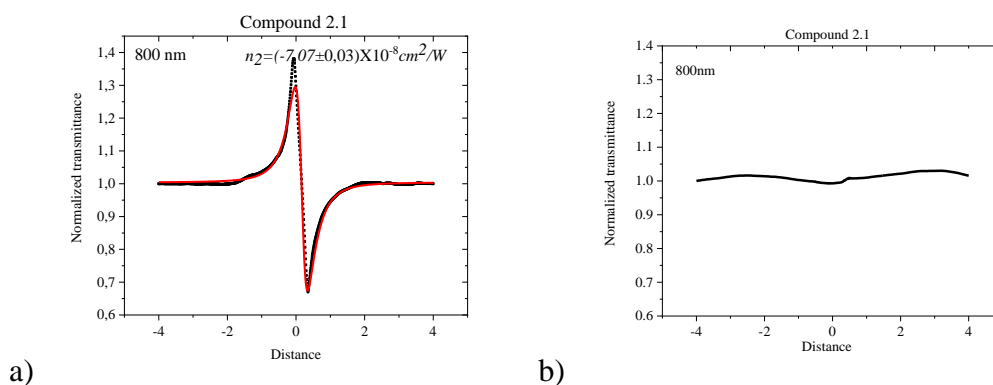


Figure 3.12 a) Closed and b) open aperture Z-scan measurement results of 0.2 mM compound 2.1 in DCM at 800 nm

From the 800 nm and 632.8 nm Z-scan measurements, nonlinear refractive index n_2 and nonlinear absorption coefficient β of compound 2.1 is extracted as $(-3.72 \pm 0.05) \times 10^{-8} \text{ cm}^2/\text{W}$ and $(-2.04 \pm 0.04) \times 10^{-8} \text{ cm}/\text{W}$ for 632.8 nm, respectively. Nonlinear refractive index n_2 of compound 1.1 is found out as $(-7.07 \pm 0.03) \times 10^{-8} \text{ cm}^2/\text{W}$ and nonlinear absorption coefficient could not be calculated at 800 nm. Compound 2.1 shows a weak response on open aperture measurements at both wavelengths. As expected, Compound 2.1 shows a stronger nonlinearity at 800 nm in closed aperture measurements. Once again this appears to be correlated with low HOMO-LUMO band gaps. In addition, the conjugation path length is smaller compared to the compound 1.1, thus the response is weaker.

3.5.4 Compound 2.2

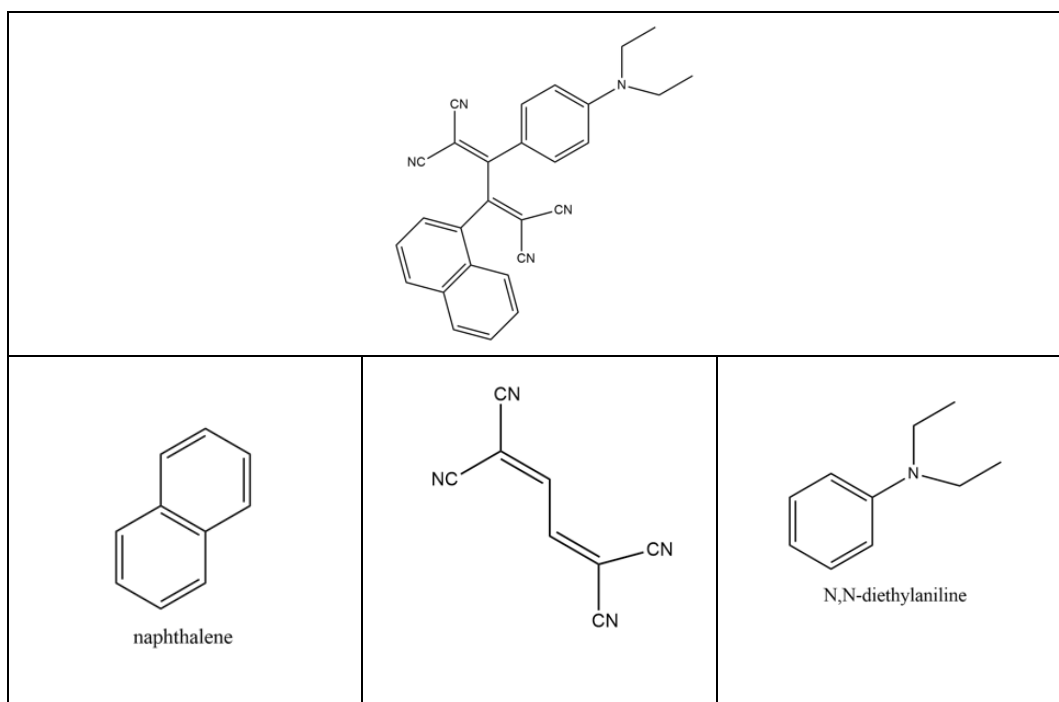


Figure 3.13 molecular fragmentation of compound 2.2

Compound 2.2 consists of diethyl aniline and naphthalene as polycyclic aromatic ring and those groups are connected to the polycyno units. Its physical structure is powder, and it's a dark-purple solid. Compound 2.2 has molar absorption coefficient of $3461 M^{-1}cm^{-1}$ at 632.8nm and of $203 M^{-1}cm^{-1}$ at 800nm. Similarly, 0.2 mM compound 2.2 in DCM was measured under 800 nm pulsed laser with 26 mW laser power and 632.8 nm He-Ne laser with 5.7 mW laser power. Normalized transmission profiles of closed and open aperture Z-scan measurements for the Compound 2.2 at both 632.8 nm and 800 nm are given in the Figure 3.15 and 3.16.

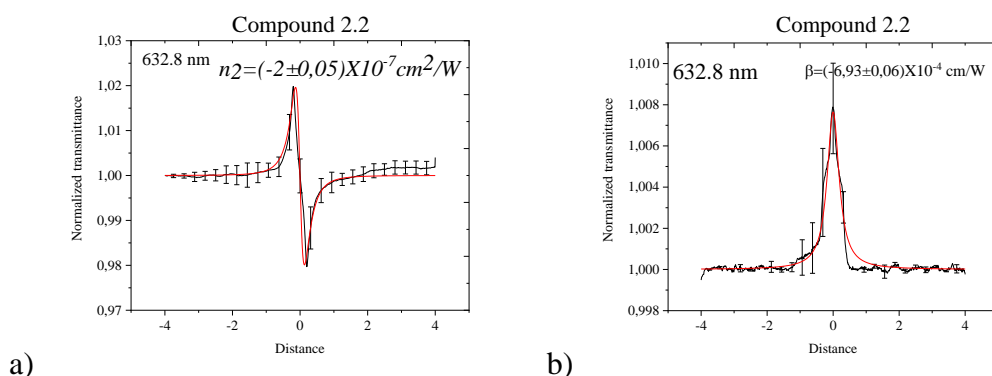


Figure 3.14 a) Closed and b) open aperture Z-scan measurement results of 0.2mM Compound 2.2 in DCM at 632.8 nm

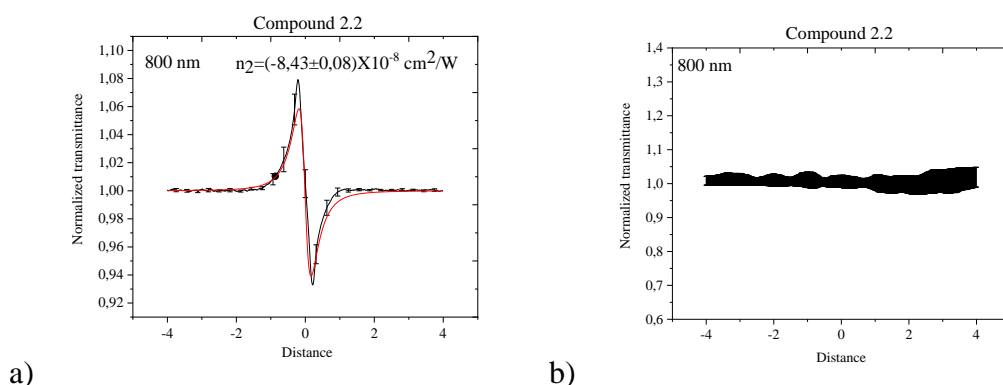


Figure 3.15 a) Closed and b) open aperture Z-scan measurements of 0.2 mM compound 2.2 in DCM at 800 nm.

With our open and closed aperture Z-scan measurements of 0.2 mM compound 2.2 nonlinear refractive index n_2 and nonlinear absorption coefficient β of compound 2.2 is figured out as $(-2.00 \pm 0.05) \times 10^{-7} \text{ cm}^2/\text{W}$ and $(-6.93 \pm 0.06) \times 10^{-4} \text{ cm}/\text{W}$ for 632.8 nm, respectively. Nonlinear refractive index of compound 2.2 is found to be $(-8.43 \pm 0.08) \times 10^{-8} \text{ cm}^2/\text{W}$ but nonlinear absorption coefficient could not be determined at 800 nm. We have observed a reasonably strong nonlinear response at 632.8 nm while almost no response at 800nm apart from nonlinear refractive index. Once again, the very weak response under 800nm laser must be related with the higher HOMO-LUMO gap and weak energy of 800nm photons. We may observe a

stronger nonlinear response at 800 nm with a high-power density at the sample, which generally results in sample damage.

3.5.5 Compound 3.1

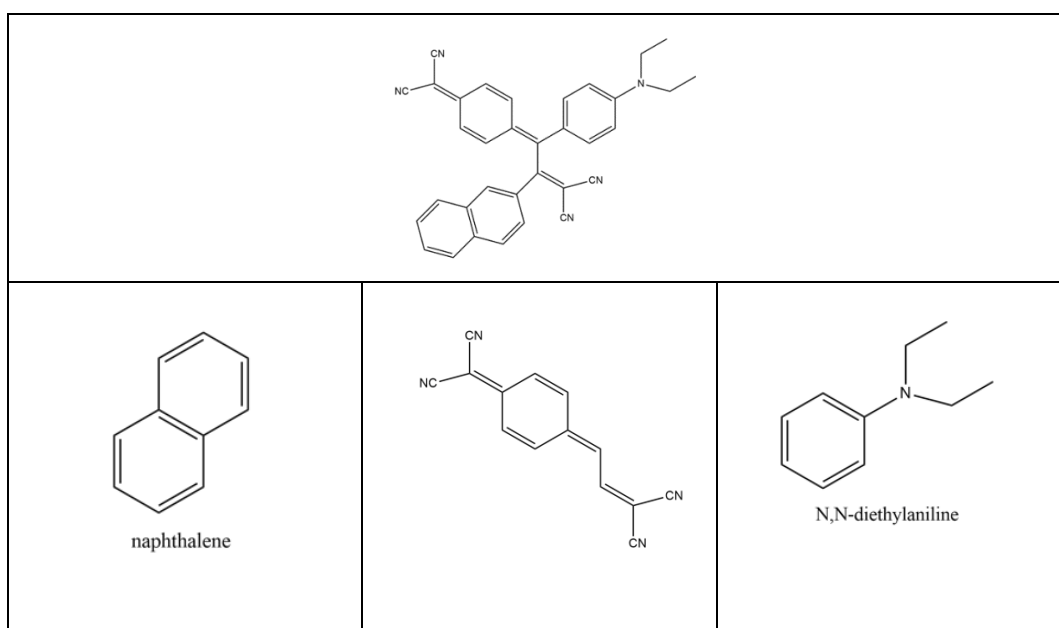
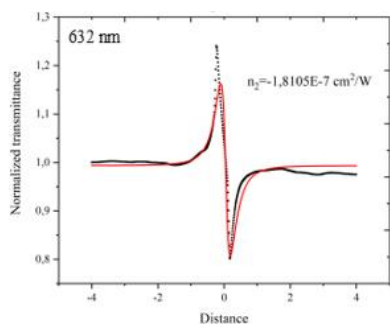
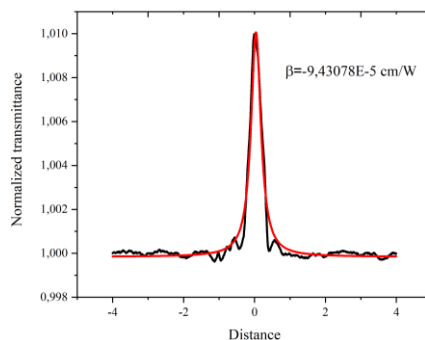


Figure 3.16 molecular fragmentation of compound 3.1

Compound 3.1 consists of diethyl aniline and naphthalene as polycyclic aromatic ring and those groups connects to the polycyno units. This is a TCNQ based. Its physical structure is powder, and its color is dark green. The Compound 3.2 has molar absorption coefficient of $11683 M^{-1}cm^{-1}$ at 800 nm and $18251 M^{-1}cm^{-1}$ at 632.8 nm. 0.2 mM Compound 3.2 in DCM was measured under 800 nm pulsed laser with 40mW laser power and 632.8 nm He-Ne laser with 5.7 mW laser power. Normalized transmission profiles of closed and open aperture Z-scan measurements for the Compound 3.2 at both 632.8 nm and 800 nm are given in Figure 3.18 and 3.19.

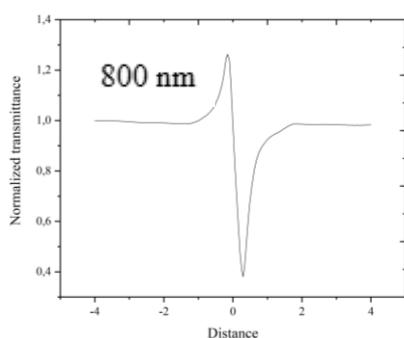


a)

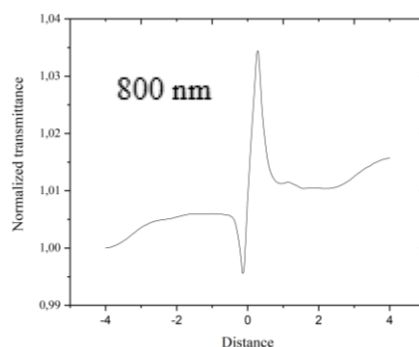


b)

Figure 3.17 a) Closed and b) open aperture Z-scan measurements of 0.2 mM Compound 3.1 in DCM at 632.8 nm



a)



b)

Figure 3.18 a) Closed and b) open aperture measurements of 0.2 mM Compound 3.1 in DCM at 800 nm

The strong nonlinear response of the Compound 3.1 was observed both with 632.8nm and 800nm lasers. The Z-scan profiles collected at 632.8nm shows us that the Compound 3.1 has both strong nonlinear absorption and nonlinear refractive index at 632.8nm. On the other hand, we have also observed a strong response under 800nm laser field, too. However, the observed profiles of closed and open aperture curves look like inverted versions of each other. The measurements were repeated at least three times. Considering quite strong 632.8 nm nonlinear responses of the Compound 3.1, which suggest strong nonlinear tensors for the compound, we think that the

observed profiles of 800nm is possibly due to the saturated response of the compound. Like other TCNQ based compounds the nonlinear response is strong. The observed behavior is correlated with the possibility of larger charge separation once the charge transfer is occurred. The results should be further investigated.

3.5.6 Compound 3.2

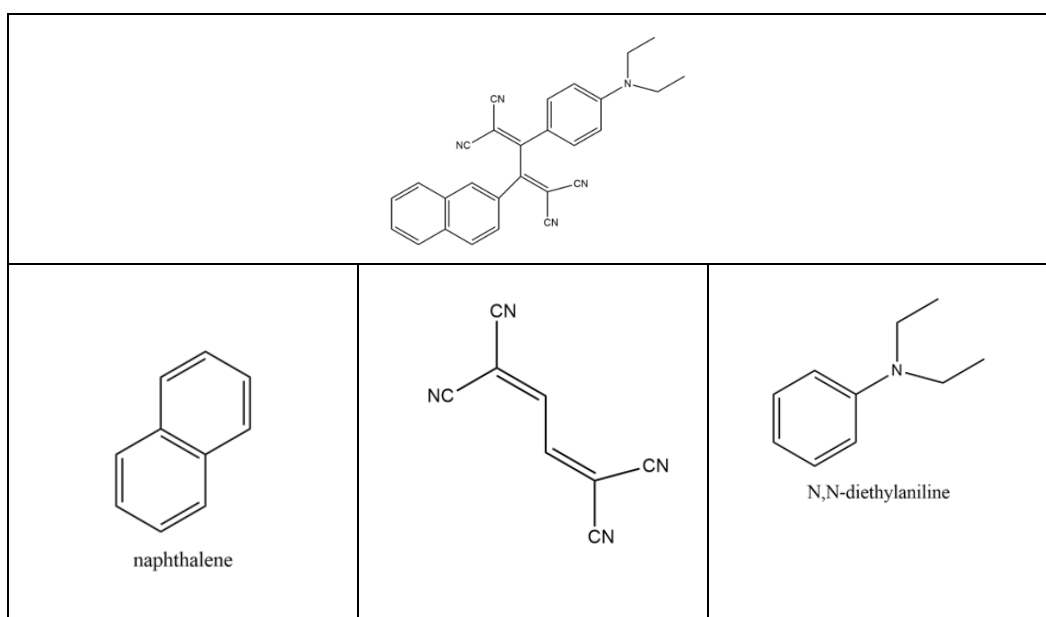
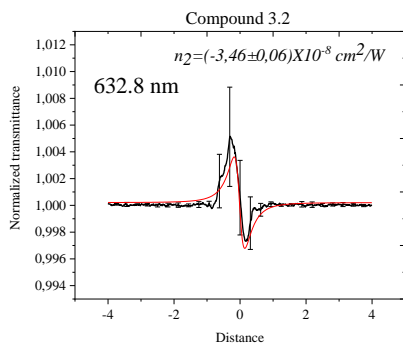
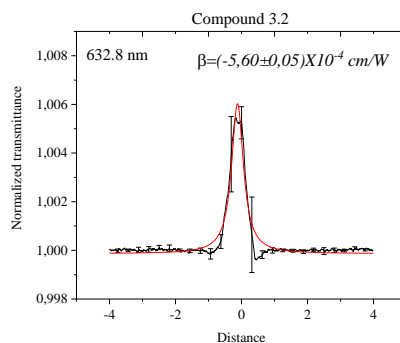


Figure 3.19 molecular fragmentation of compound 3.2

Compound 3.2 consists of diethyl aniline and naphthalene as polycyclic aromatic ring and those groups connects to the polycyno units. It has a same structure with Compound 2.2 but naphthalene link to polycyno units is from a different carbon atom. Its physical structure is powder, and its color is dark purple. Compound 3.2 has molar absorption coefficient of $739 M^{-1}cm^{-1}$ at 632.8nm and $98.5M^{-1}cm^{-1}$ at 800nm. Thus, the Compound 3.2 has comparably weaker absorption at 632.8 nm and almost no absorption at 800nm. 0.2 mM Compound 3.2 in DCM was measured under 800 nm pulsed laser with 26 mW laser power and 632.8 nm He-Ne laser with 6 mW laser power. Normalized transmission profiles of closed and open aperture Z-scan measurements for the Compound 3.2 at both 632.8 nm and 800 nm are given in the Figure 3.21 and 3.22.

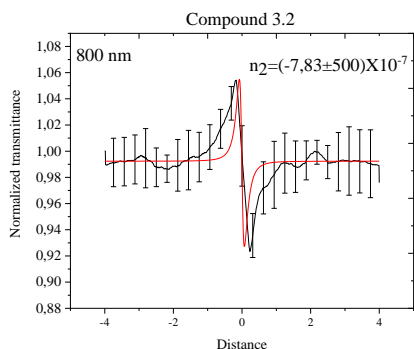


a)

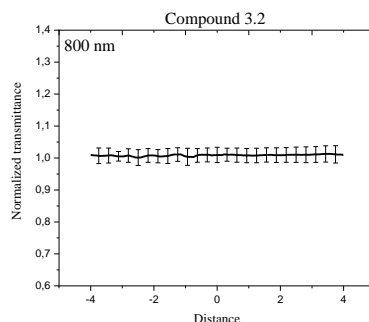


b)

Figure 3.20 a) Closed and b) open aperture Z-scan measurement result of 0.2 mM Compound 3.2 at 632.8 nm.



a)



b)

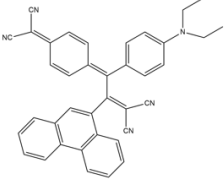
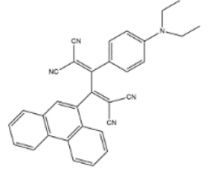
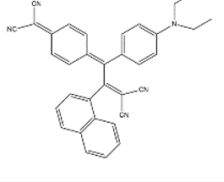
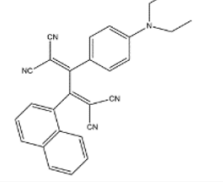
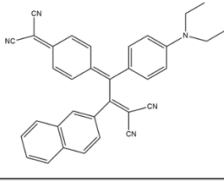
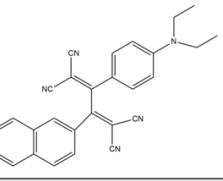
Figure 3.21 a) Closed and b) open aperture Z-scan measurement results of 0.2 mM Compound 3.2 800 nm.

Both the 632.8 and 800nm measurement results are comparably weaker than those of the other compounds, as expected. Nonlinear refractive index n_2 and nonlinear absorption coefficient β of compound 3.2 is figured out as $(-3.46 \pm 0.05) \times 10^{-8} \text{ cm}^2/\text{W}$ and $(-5.60 \pm 0.04) \times 10^{-4} \text{ cm/W}$ for 632.8 nm. On the other hand, and nonlinear refractive index n_2 of compound 3.2 is figured out as $(-7.83 \pm 500) \times 10^{-8} \text{ cm}^2/\text{W}$ but nonlinear absorption coefficient could not be calculated at 800 nm. We have not observed any nonlinear absorption response under 800 nm. Only reasonable measurement with high enough signal-to-noise is obtained with close and open aperture measurement under 632.8nm. Unfortunately, closed aperture measurement of Compound 3.2 had very low S/N ratio thus nonlinear refractive index calculation

is highly unreliable with high error. It can be about compound 3.2, because this measurement was performed after one year the compound 3.2 was synthesized. it may have deteriorated.

3.6 Comparative discussions of TCNQ and TCNE based compounds

Table 8 General view of compounds for comparison

Compound 1.1 	Compound 1.2 
Compound 2.1 	Compound 2.2 
Compound 3.1 	Compound 3.2 

In this part, nonlinear properties of the compounds will be compared. TCNQ based compounds are given in the left part of the Table 6 and are the Compound 1.1, Compound 2.1 and Compound 3.1. The TCNE compounds based are given in the right side of the Table 7 and are the Compound 1.2, the Compound 2.2 and the Compound 3.2. Thus, donor group change is down the columns while acceptor group change is across the row. Among those compound charge transfer takes place between donor diethylaniline groups to acceptor cyano groups.⁵² During comparison of their NLO responses, factors like conjugation length, aromaticity, charge transfer, HOMO-LUMO gap will be considered.

Table 8 and 9 presents the nonlinear absorption and refractive index results of the compounds at 800 nm and 632.8 nm laser measurements, respectively. We noticed that nonlinear absorption response was not observed apart from compound 1.1 and

compound 1.2 under 800 nm field, and nonlinear refractive index could not be measured for compound 3.1. The strongest response was observed for the compound 1.1 both for the nonlinear index and absorption. Given the large donor and acceptor groups and low HOMO-LUMO gap it was expected to observe the strongest response from the Compound 1.1 However, the strong nonlinear index response of the compound 3.2 was highly unexpected and could not be explained with the current information available.

All compounds showed nonlinear response under 632.8 nm laser field, and among those we have observed strongest response only for the Compound 1.1 that has maximum aromaticity due to the phenanthrene group. As expected, the nonlinear response decreased as the donor groups have changed from three rings to two ring conjugations, which increases the HOMO-LUMO gap of the TCNQ based compounds. On the other hand, we did not see such strong correlations in TCNE based compounds, even though HOMO-LUMO gap is also increasing down the group. However, the gap is already much higher than the TCNQ counterparts.

Table 9. Results of 800 nm laser measurements for every compounds

800 nm	Compound 1.1	Compound 2.1	Compound 3.1
$\beta(cm/W)$	$(-4,56\pm0,03)\times10^{-4}$	-	-
$n_2(cm^2/W)$	$(-7,29\pm0,07)\times10^{-7}$	$(-7,07\pm0,03)\times10^{-8}$	-
$M^{-1}cm^{-1}$	18819	23838	11682

Table 10 Results of 800 nm laser measurements for every compounds(con't)

800 nm	Compound 1.2	Compound 2.2	Compound 3.2
$\beta(cm/W)$	$(-7,19\pm0,05)\times10^{-5}$	-	-
$n_2(cm^2/W)$	$(-4,61\pm0,04)\times10^{-8}$	$(-8,43\pm0,08)\times10^{-8}$	$(-7,83,\pm500)\times10^{-7}$
$M^{-1}cm^{-1}$	147.03	203.60	98.504

Table 11. Results of 632.8 nm laser measurements for every compounds

632.8 nm	Compound 1.1	Compound 2.1	Compound 3.1
$\beta(cm/W)$	$(-7,06\pm0,05)\times10^{-4}$	$(-2,04\pm0,04)\times10^{-8}$	$(-9,43)\times10^{-5}$
$n_2(cm^2/W)$	$(-6,30\pm0,05)\times10^{-7}$	$(-3,72\pm0,05)\times10^{-8}$	$(-1,81)\times10^{-7}$
$M^{-1}cm^{-1}$	9966.4	14762	18251

632.8 nm	Compound 1.2	Compound 2.2	Compound 3.2
$\beta(cm/W)$	$(-3,37\pm0,02)\times10^{-6}$	$(-6,93\pm0,06)\times10^{-4}$	$(-5,60\pm0,05)\times10^{-4}$
$n_2(cm^2/W)$	$(-2,70\pm0,03)\times10^{-7}$	$(-2,00\pm0,05)\times10^{-7}$	$(-3,46,\pm0,06)\times10^{-8}$
$M^{-1}cm^{-1}$	4460.1	3460.8	738.79

The Compound 1.1 as a TCNQ based compound has most electron rich aromatic ring groups among all other compounds due to the long pi-bond chain in phenanthrene. In addition, the Compound 1.1 has a longer pi delocalization within the acceptor group compared to the Compound 1.2. This leads to an increase in possible number of resonance structures and results in intense and stable charge transfer property.

This is possibly one of the reasons that the Compound 1.1 showed largest experimental nonlinear refractive index and nonlinear absorption coefficient values among all compounds. This is consistent with the theoretical calculations and recently reported results on a study by Dengiz et. al⁵². In the study, it has been observed that compound 1.1 has high hyperpolarizability value.

When compound 2.1 and compound 2.2 are considered, again the only difference is the TCNQ group that increase the pi bonding (see Table 7). Therefore, it is expected that it should show better NLO response then the compound 2.2 as observed between the compounds 1.1 and 1.2. However, according to experimental results obtained with 632.8 nm measurements, the Compound 2.2 showed a better NLO response, especially when nonlinear absorptions are compared. Here we have to note that strong linear absorption of 632.8 nm light by the compound 2.1 may have affected the observed nonlinear behavior since the photon number is highly limited at 632.8nm (only 5 mW). On the other hand, nonlinear refractive index of the compounds both at 800nm and 632.8 nm appears to be quite similar. This brings a question regarding the effect of HOMO-LUMO gap on the NLO response of the compounds.

A similar difference exists between the Compound 3.1 and the Compound 3.2 where only the acceptor is changed. Considering the pi delocalization, it is expected that compound 3.1 should show better NLO response compared to the Compound 3.2. However, when compound 3.1 have better nonlinear refractive index value than compound 3.2, compound 3.2 have better nonlinear absorption coefficient value for 632.8 nm field. Once again it should be noted that the linear absorption of 3.1 at 632.8nm is much higher than the compound 3.2.

The Compound 2.1 and the Compound 3.1 or the Compound 2.2 and the Compound 3.2 do only vary in structure due to the linkage point of the naphthalene group (see Table 7) While the naphthalene is connected from the 1st carbon on the Compound 2.1 and the compound 2.2 it is connected from the 3rd carbon in the compound 3.1 and the compound 3.2. According to the Z-scan analysis of these samples, naphthalene that is bonded from the 3rd carbon shows better NLO response rather

than naphthalene that is bonded from 1st. It can be about distance between naphthalene pi bonds and acceptor cyano groups. For case where it is connected from the 1st carbon, naphthalene pi bonds are closer to the cyano group and during charge transfer, electrons that belongs to naphthalene can conflict with the electrons that comes from the aniline, and they can push each other, and it makes charge transfer harder that leads to decrease in the NLO response. On the other hand, such coordination of the naphthalene group may increase the hyperpolarizability of the compounds, resulting a better nonlinear response.

In addition to that, the HOMO-LUMO gap expected to have important role in the nonlinear optical properties of compounds. If HOMO-LUMO gap is small, since energy barrier that electron can be transferred is small, charge transfer become easier and NLO response is expected to increase⁵⁷.

In those compounds, while HOMO is located on the diethylaniline, LUMO is located on cyano groups. The HOMO-LUMO gap energies reported for these compounds in reference 52 is given in Table 11.

Table 12. HOMO-LUMO gap energies

TCNQ based compounds		TCNE based compounds	
Compound 1.1	1.73 eV	Compound 1.2	2.28 eV
Compound 2.1	1.72 eV	Compound 2.2	2.30 eV
Compound 3.1	1.87 eV	Compound 3.2	2.57 eV

HOMO-LUMO gap energy of the TCNQ based compounds is smaller than the TCNE compounds. Therefore, it is expected that all the TCNQ compounds would show a better NLO response than the TCNE counter parts. However, in experimental results, although the Compound 2.2 is TCNE based compounds, it has strong NLO response compared to the Compound 2.1 that have a smaller HOMO-LUMO gap. On the other hand, the Compound 3.2 has the biggest HOMO-LUMO gap, and its nonlinear absorption coefficient could not be measured at 800 nm field In contrast, the Compound 1.1 and the Compound 1.2 have very

similar HOMO-LUMO gap, but we have only observed a strong nonlinear response for the Compound 1.1. Since, there are many factors that affects the nonlinear optical properties, it can be said that, there is indirect relation between HOMO-LUMO gap and nonlinear optical properties. Further investigation of the HOMO-LUMO effect on the nonlinear response needs to be carried out.

3.7 Additional studies

In addition to the presented work, the study is expanded to include further TCNQ and TCNE based compounds where especially the donor groups were changed to smaller groups. To further investigate different donor group effect on the nonlinear refractive index and nonlinear absorption coefficient in such donor-acceptor systems. Similar to the previous case, measurements were performed with 5.7 mW He-Ne laser beam in solution form with 1mm thick quartz cuvette at beam intensity of ca. 300 W/cm² at the focal point. This cuvette was translated through laser beam path via motorized stage that has certain speed and accuracy. Organic solutions were prepared as 0.2 M by dissolving them in Dichloromethane (DCM). Nonlinear absorption and refractive index measurements for TCNQ compounds were performed with both open aperture and closed aperture. To provide same measurement conditions the same pin hole was used for all closed aperture measurements.

, All these comes about are supporting that there's ICT and productive charge-separation in particles. In this concept, there are 6 different Donor-acceptor (D- π -A) push-pull chromophore systems and difference between those system is donor group. Since different donor groups has different donor abilities,⁴¹ this way it might be possible to shed more light onto the donor effect on nonlinear optical properties. Affect All measurements are illustrated in Figure 3.23 and Figure 3.24. While graph at left columns shows open aperture measurements (enables to calculate nonlinear absorbance coefficient), graph at right columns shows closed aperture measurements, which enables to calculate nonlinear refractive index.

In Figure 3.23, Nonlinear absorption coefficient and nonlinear refractive index measurements of TCNQ based compounds were illustrated, and results are given in Table 12. Nonlinear absorption and nonlinear refractive index of those compounds were calculated as benzothiazole **122** ($\beta = -8.12 \times 10^{-4} \text{ cm W}^{-1}$, $n^2 = -1.94 \times 10^{-7} \text{ cm}^2 \text{ W}^{-1}$), quinoline **124** ($\beta = -7.03 \times 10^{-4} \text{ cm W}^{-1}$, $n^2 = -2.26 \times 10^{-6} \text{ cm}^2 \text{ W}^{-1}$), and pyridine **125** ($\beta = -9.90 \times 10^{-4} \text{ cm W}^{-1}$, $n^2 = -7.54 \times 10^{-7} \text{ cm}^2 \text{ W}^{-1}$). When results are compared by looking by HOMO-LUMO gap, results are compatible with HOMO-LUMO gap of compounds, However, there is indirect relationship between HOMO-LUMO gap and nonlinear optical properties. In addition to that, electron-donating ability is directly related with nonlinear optical respond. As reported in the literature, strong donor ability enhances the nonlinear optical properties because probability of intermolecular charge transfer (ICT) is also increased.⁴² Upon that, when order of the donor ability of utilized donor group is regarded, Quinoline has strong donor between other donor groups because quinoline has the strong red shift that makes donor ability stronger, than benzothiazole. Donor ability of benzothiazole stronger than the pyridine due to the strong red shift of benzothiazole. Therefore, it is expected that the order of the nonlinear optical response of the compounds should be **124>122>125**. While nonlinear index did follow the trend where the compound 124 has the highest nonlinear index value; however, the nonlinear absorption coefficients did not follow this trend. This is possibly again due to the limited low power of 632.8nm laser and linear absorption coefficient differences of these compounds.

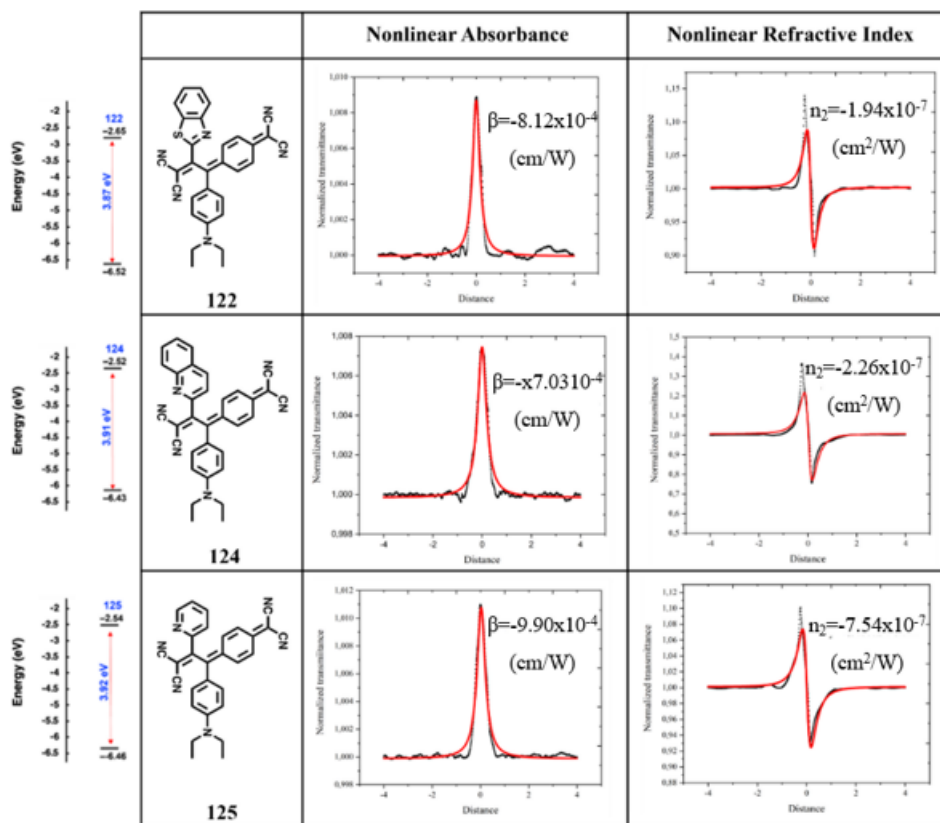


Figure 3.22 Nonlinear absorption and refractive index measurements of TCNQ attached NLOphres

Table 13. Nonlinear absorption and refractive index values of TCNQ attached NLOphres.

Compound number	β (cm/W)	n_2 (cm ² /W)
122	-8.12×10^{-4}	-1.94×10^{-7}
124	-7.03×10^{-4}	-2.26×10^{-6}
125	-9.90×10^{-4}	-7.54×10^{-7}

Similarly, nonlinear absorption and refractive index measurements of TCNE attached NLOphres were performed and is illustrated in Figure 3.24 and the results are presented in Table 13. Nonlinear absorption and refractive index of compounds

were calculated as benzimidazole **112** ($\beta = -1.43 \times 10^{-4} \text{ cm/W}$, $n^2 = -1.59 \times 10^{-7} \text{ cm}^2/\text{W}$), benzothiazole **115** ($\beta = -7.35 \times 10^{-4} \text{ cm/W}$, $n^2 = -3.55 \times 10^{-7} \text{ cm}^2/\text{W}$), and thiophene **116** ($\beta = -2.36 \times 10^{-4} \text{ cm/W}$, $n^2 = -1.65 \times 10^{-8} \text{ cm}^2/\text{W}$). Since compound **116** have bigger HOMO-LUMO gap it is expected that it should have the smallest nonlinear response than the compounds **115** and **112**.

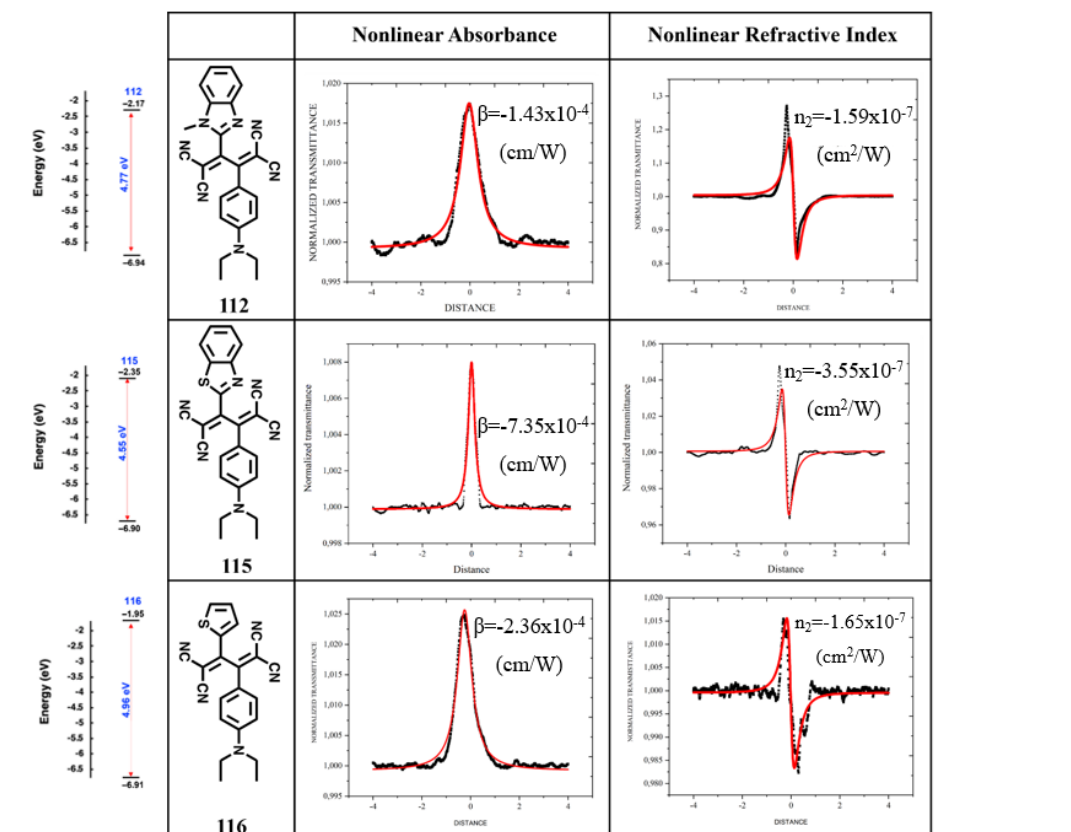


Figure 3.23 Nonlinear absorption and refractive index measurements of TCNE attached NLOphres

Table 14. Nonlinear absorption and refractive index values of TCNE attached NLOphores.

Compound number	$\beta(\text{cm/W})$	$n_2 (\text{cm}^2/\text{W})$
112	-1.43×10^{-4}	-1.59×10^{-7}
115	-7.35×10^{-4}	-3.55×10^{-7}
116	-2.36×10^{-4}	-1.65×10^{-8}

However, its nonlinear absorption coefficient is bigger than compound **115** but is smaller than the compound **112**. Though, all are very close to each other. It can be about having greater donor ability of thiophene than benzothiazole. On the other hand, the nonlinear index appears to follow the trend and the Compound **116** has the weakest response.

CHAPTER 4

CONCLUSION

In this thesis study, basic and efficient Z-scan technique was chosen as method to investigate the nonlinear optical behavior of TCNE and TCNQ based compounds. In the first part of the study, a Z-Scan optical setup was constructed successfully. Next, the operation and validation of the collected data with the setup was tested by measuring nonlinear properties of known chemicals (tungsten disulfide and methylene blue) obtained from literature. Slight deviations of the nonlinear absorption coefficient and the nonlinear index measured with our setup were attributed to the differences in preparation of the films, the concentration of the solutions or the fitting parameters due to differences in laser characteristics. The results are very close and confirm the successful construction of the setup. In addition, during construction of the optical setup, I have gained experiences on usage of optics, optomechanical parts, building an optical system, and controlling motorized translational stage with Arduino and MATLAB. After the successful construction of the setup, data acquisition chain was established and processing and data fitting with equation enabled extraction of the nonlinear properties from the measurements.

In the second part of the study, nonlinear responses of TCNE and TCNQ based compounds were measured with 800nm laser and 632.8nm laser and presented. Measurements enabled extraction of nonlinear absorption coefficients and nonlinear refractive index values of these compounds. Repeatability and measurement errors are determined by repeating the measurements five times. These compounds have good donor and acceptor components with high conjugations thus expected to show strong nonlinear responses. Depending on the laser color used, we have observed strong responses from each of these compounds. Due to its low energy compared to the 632.8nm laser color we could not extract the nonlinear properties of some of the

compounds at 800nm, especially for TCNE based compounds. In general, we noticed that conjugation length has strong effect on the observed nonlinear behaviour. For example, nonlinear optical property increased for Compound 1.1 compared to Compound 1.2. However, we need to mention that this statement was not valid when we compare the Compound 2.1 and Compound 2.2. Therefore, it was concluded that there is no direct relation between conjugation length and nonlinear optical properties. Moreover, it was concluded that bonding location of naphthalene on the compounds (i.e., Compound 2.1 and Compound 2.2 or Compound 3.1 and Compound 3.2) has also effect on nonlinear optical properties. It is noticed that HOMO-LUMO gap has an indirect relation to the nonlinear optical properties. As a conclusion we have seen strong correlation with the donor and the acceptor abilities of a compound to its nonlinear properties. As a result, TCNQ based compounds have better nonlinear responses than TCNE based compounds.

REFERENCES

1. Zhong, Q. & Fourkas, J. T. Optical Kerr Effect Spectroscopy of Simple Liquids †. 15529–15539 (2008).
2. Busch, G. Early history of ferroelectricity. *Ferroelectrics* **74**, 267–284 (1987).
3. Semin, S., Li, X., Duan, Y. & Rasing, T. Nonlinear Optical Properties and Applications of Fluorenone Molecular Materials. *Adv. Opt. Mater.* **9**, (2021).
4. Yin, J. *et al.* A new stilbazolium salt with perfectly aligned chromophores for second-order nonlinear optics: 4-N,N-Dimethylamino-4'-N'-methylstilbazolium 3-carboxy-4-hydroxybenzenesulfonate. *Dye. Pigment.* **94**, 120–126 (2012).
5. Feng, M., Zhan, H. & Chen, Y. Nonlinear optical and optical limiting properties of graphene families. *Appl. Phys. Lett.* **96**, 2010–2013 (2010).
6. Marder, S. R. Organic nonlinear optical materials: Where we have been and where we are going. *Chem. Commun.* 131–134 (2006)
doi:10.1039/b512646k.
7. Steinmann, C. Development and characterisation of a tunable laser source in the vacuum ultraviolet. (1999).
8. Yan, X.-Q., Liu, Z.-B., Zhang, X.-L., Zhou, W.-Y. & Tian, J.-G. Polarization dependence of Z-scan measurement: theory and experiment. *Opt. Express* **17**, 6397 (2009).
9. Stolle, R., Marowsky, G., Schwarzberg, E. & Berkovic, G. Phase measurements in nonlinear optics. *Appl. Phys. B Lasers Opt.* **63**, 491–498 (1996).
10. Franken, P. A., Hill, A. E., Peters, C. W. & Weinreich, G. Generation of optical harmonics. *Phys. Rev. Lett.* **7**, 118–119 (1961).
11. Klein, M. W., Enkrich, C., Wegener, M. & Linden, S. Second-harmonic

- generation from magnetic metamaterials. *Science* (80-.). **313**, 502–504 (2006).
12. Neethling, P. H. Determining non-linear optical properties using the Z-scan technique. (2005).
 13. Ewart, P. mask for the imaging of thin-layer chromatography plates by laser-induced fluorescence or surface-enhanced Raman scattering and for use with a. 109–119 (2002).
 14. Ananthi, N., Balakrishnan, U., Velmathi, S., Manjunath, K. B. & Umesh, G. Synthesis, Characterization and Third Order Non Linear Optical Properties of Metallo Organic Chromophores. *Opt. Photonics J.* **02**, 40–45 (2012).
 15. ACTIVE PHOTONIC DEVICES BASED ON LIQUID CRYSTALS. (2013).
 16. Wang, G., Baker-Murray, A. A. & Blau, W. J. Saturable Absorption in 2D Nanomaterials and Related Photonic Devices. *Laser Photonics Rev.* **13**, 1–23 (2019).
 17. Wang, L. & Men, Y. Comparison study of CsLiB₆O₁₀ and. **2**, 10–13 (2003).
 18. Chen, S. *et al.* Broadband optical and microwave nonlinear response in topological insulator. *Opt. Mater. Express* **4**, 587 (2014).
 19. Medishetty, R., Zaręba, J. K., Mayer, D., Samoć, M. & Fischer, R. A. Nonlinear optical properties, upconversion and lasing in metal-organic frameworks. *Chem. Soc. Rev.* **46**, 4976–5004 (2017).
 20. Materials, T. O. Высокоэффективная Электрооптическая Полупроводниковая Среда На Основе Гетероструктур Второго Рода. ‘*Физика И Техника Полупроводников*’ **47**, 1542 (2013).
 21. Weaire, D., Wherrett, B. S., Miller, D. A. B. & Smith, S. D. Effect of low-power nonlinear refraction on laser-beam propagation in InSb. *Opt. Lett.* **4**,

- 331 (1979).
22. Sheik-Bahae, M, Said, A.A., Van Stryland, E. W. *Opt. Lett.* **14**, 955 (1989).
 23. Stegeman, G. I. *et al.* Modification to the z-scan technique by widths measurements. *Opt. Express* **274**, 83–86 (2005).
 24. Stegeman, G. I., Sheik-Bahae, M., Van Stryland, E. & Assanto, G. Large nonlinear phase shifts in second-order nonlinear-optical processes. *Opt. Lett.* **18**, 13 (1993).
 25. Reynaud, F., Salin, F. & Barthelemy, A. Measurement of phase shifts introduced by nonlinear optical phenomena on subpicosecond pulses. *Opt. Lett.* **14**, 275 (1989).
 26. Rekha, R. K. & Ramalingam, A. Non-linear characterization and optical limiting effect of carmine dye. *Indian J. Sci. Technol.* **2**, (2009).
 27. Liu, X., Guo, S., Wang, H., Ming, N. & Hou, L. Investigation of the influence of finite aperture size on the z-scan transmittance curve. *J. Nonlinear Opt. Phys. Mater.* **10**, 431–439 (2001).
 28. PALFFY-MUHORAY, P. Z-Scan Measurements of Optical Nonlinearities of Liquid Crystals. *Phase Transitions in Complex Fluids* 429–444 (1998) doi:10.1142/9789812816825_0017.
 29. Ghezelbash, Z. D., Motiei, H., Mahmoody, M. & Dilmaghani, K. A. Synthesis, characterization, and nonlinear optical properties of some new series of S-(5-aryl-1,3,4-oxadiazol-2-yl) 2-chloroethanethioate derivatives. *Turkish J. Chem.* **43**, 902–910 (2019).
 30. Henari, F. Z. & Patil, P. S. Nonlinear Optical Properties and Optical Limiting Measurements of {(1Z)-[4-(Dimethylamino)Phenyl]Methylene} 4-Nitrobenzocaroxy Hydrazone Monohydrate under CW Laser Regime. *Opt. Photonics J.* **04**, 182–188 (2014).

31. Datta, A. & Pal, S. Effects of conjugation length and donor-acceptor functionalization on the non-linear optical properties of organic push-pull molecules using density functional theory. *J. Mol. Struct. THEOCHEM* **715**, 59–64 (2005).
32. Sajan, D., Vijayan, N., Safakath, K., Philip, R. & Joe, I. H. Intramolecular charge transfer and Z-scan studies of a semiorganic nonlinear optical material sodium acid phthalate hemihydrate: A vibrational spectroscopic study. *J. Phys. Chem. A* **115**, 8216–8226 (2011).
33. Vijayalakshmi, S. & Kalyanaraman, S. Role of charge transfer on the nonlinear optical properties of donor- π -acceptor (D- π -a) conjugated Schiff bases with DFT approach. *J. Phys. Org. Chem.* **29**, 436–442 (2016).
34. Abbotto, A. *et al.* A distinctive example of the cooperative interplay of structure and environment in tuning of intramolecular charge transfer in second-order nonlinear optical chromophores. *Chem. - A Eur. J.* **9**, 1991–2007 (2003).
35. Hegde, T. A., Dutta, A., Girisun, T. C. S. & Vinitha, G. A novel chlorocadmite hybrid cocrystal delivering intermolecular charge transfer enhanced nonlinear optical properties and optical limiting. *Opt. Mater. (Amst)*. **117**, 111194 (2021).
36. Ali, B. *et al.* Key electronic, linear and nonlinear optical properties of designed disubstituted quinoline with carbazole compounds. *Molecules* **26**, (2021).
37. Pearson, R. G. Absolute electronegativity and hardness correlated with molecular orbital theory. *Proc. Natl. Acad. Sci.* **83**, 8440–8441 (1986).
38. Taherpour, A. Structural relationship between degree of unsaturation with Fermi energy, chemical hardness, and the HOMO-LUMO gap of (5,5) armchair single-walled carbon nanotubes. *Fullerenes Nanotub. Carbon Nanostructures* **17**, 26–37 (2009).

39. Acharya, S. & Rebarry, B. Study on the interaction of 3,4-dihydroxyphenylalanine (DL-DOPA) with nonionic and ionic surfactants by fluorescence and UV-visible spectroscopy. *J. Surf. Sci. Technol.* **26**, 95–103 (2010).
40. Jia, J. *et al.* Effect of intramolecular charge transfer on nonlinear optical properties of chalcone derivatives: a visual description of the charge transfer process. *Phys. Chem. Chem. Phys.* **24**, 955–965 (2022).
41. Huang, T. H. *et al.* Linear and nonlinear optical properties of two novel D- π -A- π -D type conjugated oligomers with different donors. *Opt. Mater. (Amst)*. **35**, 467–471 (2013).
42. Shen, Y., Chen, P., Liu, J., Ding, J. & Xue, P. Effects of electron donor on luminescence and mechanochromism of D- π -A benzothiazole derivatives. *Dye. Pigment.* **150**, 354–362 (2018).
43. Batista, R. M. F., Costa, S. P. G., Belsley, M. & Raposo, M. M. M. Synthesis and second-order nonlinear optical properties of new chromophores containing benzimidazole, thiophene, and pyrrole heterocycles. *Tetrahedron* **63**, 9842–9849 (2007).
44. Essam, Z. M. *et al.* Donor acceptor fluorophores: synthesis, optical properties, TD-DFT and cytotoxicity studies. *Org. Biomol. Chem.* **19**, 1835–1846 (2021).
45. Khalid, M. *et al.* Electron donor and acceptor influence on the nonlinear optical response of diacetylene-functionalized organic materials (DFOMs): Density functional theory calculations. *Molecules* **24**, (2019).
46. Zin, S. Y., Cho, D. G., Kil, S. K., Sessler, J. L. & Kim, D. Nonlinear optical properties as a guide to aromaticity in congeneric pentapyrrolic expanded porphyrins: Pentaphyrin, sapphyrin, isosmaragdyrin, and orangarin. *J. Am. Chem. Soc.* **130**, 6930–6931 (2008).
47. Wang, Z. *et al.* Novel Third-Order Nonlinear Optical Materials with Craig-

- Möbius Aromaticity. *J. Phys. Chem. Lett.* **12**, 11784–11789 (2021).
48. Ali, Q. M. & Palanisamy, P. K. Investigation of nonlinear optical properties of organic dye by Z-scan technique using He-Ne laser. *Optik (Stuttg.)* **116**, 515–520 (2005).
 49. Wei, R. *et al.* Facile synthesis of two-dimensional WS₂ with reverse saturable absorption and nonlinear refraction properties in the PMMA matrix. *J. Alloys Compd.* **684**, 224–229 (2016).
 50. Zheng, X. *et al.* Z-scan measurement of the nonlinear refractive index of monolayer WS₂. *Opt. Express* **23**, 15616 (2015).
 51. Jiang, G. Q., Yao, C. B., Bao, S. Bin & Cai, Y. Standing growth mechanism and ultrafast nonlinear absorption properties of WS₂ films. *Opt. Mater. (Amst.)* **106**, 109995 (2020).
 52. Primer, M. & Techniques, S. M. The Quarter Wavelength Retardation Plate. 3–5 (2023).
 53. Jaffar, A. F. Solvent Effect on the Third Order nonlinearity of Oxazine Dye Doped PMMA Films by Using Z-Scan Techniques. (2020).
 54. Taheri, B. *et al.* Intensity scan and two photon absorption and nonlinear refraction of C 60 in toluene. *Appl. Phys. Lett.* **1317**, 1317 (1995).
 55. Jeyara, S. Study of third-order nlo properties of organic dye for optoelectronics applications. *Optoelectron. Adv. Mater. Rapid Commun.* **15**, 62–66 (2021).
 56. Dengiz, Ç. Polycyclic aromatic hydrocarbon-substituted push-pull chromophores: An investigation of optoelectronic and nonlinear optical properties using experimental and theoretical approaches. *Turkish J. Chem.* **45**, 1375–1390 (2021).
 57. Hadji, D. & Rahmouni, A. Theoretical study of nonlinear optical properties of some azoic dyes. *Mediterr. J. Chem.* **4**, 185–192 (2015).

